

AD-A245 926



NAVAL POSTGRADUATE SCHOOL Monterey, California



THESIS

VISUALIZATION OF GAS TUNGSTEN
ARC WELD POOLS

by

Daniel C. Espinosa

SEPTEMBER 1991

Thesis Advisor:

Yogendra Joshi

Approved for public release: Distribution is unlimited

92 2 12 199

92-03702



Unclassified

SECURITY CLASSIFICATION OF THIS PAGE

REPORT DOCUMENTATION PAGE				Form Approved OMB No 0704-0188	
1a. REPORT SECURITY CLASSIFICATION Unclassified			1b. RESTRICTIVE MARKINGS		
2a. SECURITY CLASSIFICATION AUTHORITY			3. DISTRIBUTION/AVAILABILITY OF REPORT Approved for public release: Distribution is unlimited		
2b. DECLASSIFICATION/DOWNGRADING SCHEDULE					
4. PERFORMING ORGANIZATION REPORT NUMBER(S)			5. MONITORING ORGANIZATION REPORT NUMBER(S)		
6a. NAME OF PERFORMING ORGANIZATION Naval Postgraduate School		6b. OFFICE SYMBOL (If applicable) ME		7a. NAME OF MONITORING ORGANIZATION Naval Postgraduate School	
6c. ADDRESS (City, State and ZIP Code) Monterey, CA 93943-5000			7b. ADDRESS (City, State, and ZIP Code) Monterey, CA 93943-5000		
8a. NAME OF FUNDING/SPONSORING ORGANIZATION		8b. OFFICE SYMBOL (If applicable)		9. PROCUREMENT INSTRUMENT IDENTIFICATION NUMBER	
8c. ADDRESS (City, State, and ZIP Code)			10. SOURCE OF FUNDING NUMBER		
			PROGRAM ELEMENT NO.	PROJECT NO.	TASK NO.
			WORK UNIT ACCESSION NO.		
11. TITLE (Include Security Classification) VISUALIZATION OF GAS TUNGSTEN ARC WELD POOLS					
12. PERSONAL AUTHORS DANIEL C. ESPINOSA					
13a. TYPE OF REPORT Master's Thesis		13b. TIME COVERED FROM _____ TO _____		14. DATE OF REPORT (Year, Month, Day) SEPTEMBER 1991	
				15. PAGE COUNT 83	
16. SUPPLEMENTARY NOTATION The views expressed are those of the author and do not reflect the official policy or position of the Department of Defense or the U.S. Government					
17. COSATI CODES			18. SUBJECT TERMS (Continue on reverse if necessary and identify by block numbers)		
FIELD	GROUP	SUB-GROUP	gas tungsten welding, visualization, weld pools		
19. ABSTRACT (Continue on reverse if necessary and identify by block numbers) Surface flow visualization of Gas Tungsten Arc weld pools for HY-80 steel is presented using a pulsed laser light source and a conventional night vision image-intensifier tube equipped video camera. Visualization of the weld pool free surface is made possible by seeding the flow with alumina particles for both stationary and moving arc welds. These visualizations reveal several new features not incorporated in the existing models for stationary welds. A strong clockwise stirring is observed contrary to the axisymmetric computational models. Also, the pool surface shows a bulge near the center. Complex flow patterns are observed for moving arc welding. Interpretations of the observed flows based on the driving forces are provided.					
20. DISTRIBUTION/AVAILABILITY OF ABSTRACT <input checked="" type="checkbox"/> UNCLASSIFIED/UNLIMITED <input type="checkbox"/> SAME AS RPT <input type="checkbox"/> DTIC USERS			21. ABSTRACT SECURITY CLASSIFICATION Unclassified		
22a. NAME OF RESPONSIBLE INDIVIDUAL Yogendra Joshi			22b. TELEPHONE (Include Area Code) (408) 646-3400		22c. OFFICE SYMBOL ME/Ji

Approved for public release: Distribution is unlimited

Visualization of Gas Tungsten Arc Weld Pools

by

Daniel C. Espinosa
Lieutenant, United States Navy
B.A., University of New Mexico, Chemistry, 1985

Submitted in partial fulfillment of the
requirements for the degree of

MASTER OF SCIENCE IN
MECHANICAL ENGINEERING

from the


NAVAL POSTGRADUATE SCHOOL

SEPTEMBER 1991

Author:


Daniel C. Espinosa

Approved by:


Yogendra Joshi, Thesis Advisor


A.J. Healey, Chairman
Department of Mechanical Engineering

ABSTRACT

Surface flow visualization of Gas Tungsten Arc weld pools for HY-80 steel is presented using a pulsed laser light source and a conventional night-vision image-intensifier tube equipped video camera. Visualization of the weld pool free surface is made possible by seeding the flow with alumina particles for both stationary and moving arc welds. These visualizations reveal several new features not incorporated in the existing models for stationary welds. A strong clockwise stirring is observed contrary to the axi-symmetric computational models. Also, the pool surface shows a bulge near the center. Complex flow patterns are observed for moving arc welding. Interpretations of the observed flows based on the driving forces are provided.

Accession For	
NTIS CRA&I	<input checked="" type="checkbox"/>
DTIC TAB	<input type="checkbox"/>
Unannounced	<input type="checkbox"/>
Justification	
By	
Distribution/	
Availability Codes	
Dist	Availability for Special
A-1	



TABLE OF CONTENTS

I.	INTRODUCTION	1
	A. SELECTED HISTORY OF NUMERICAL INVESTIGATIONS	1
	B. SELECTED HISTORY OF EXPERIMENTAL INVESTIGATIONS	5
	C. PRESENT EXPERIMENTAL INVESTIGATION	9
II.	EXPERIMENTAL SET-UP AND PROCEDURE	11
	A. GAS TUNGSTEN ARC WELDING APPARATUS	11
	B. MATERIAL CHARACTERISTICS	11
	C. WELD POOL VISUALIZATION SYSTEM	12
	1. Laser	13
	2. Vision System	13
	3. Monitor and Recording	15
	D. EXPERIMENTAL PROCEDURE	16
	1. Sample Preparation	16
	2. Vision System Preparation	16
	3. Welding Equipment	17
III.	STATIONARY ARC EXPERIMENTS	18
	A. WELDING EFFICIENCY	18
	B. GROUNDING EFFECTS	21
	C. WELD POOL DEVELOPMENT	26
	1. Effect of Input Power Changes	26
	2. Effect of Arc Length Changes	32
	3. Effects of Electrode Tip Angle	32
	D. WELD POOL OBSERVATIONS	34
	1. Weld Pool Rise	34
	2. Flow Observations	36
	3. Weld Pool Oscillations	40
IV.	MOVING ARC EXPERIMENTS	43
	A. WELDING EFFICIENCY	43
	B. EFFECT OF WELDING POWER	48
	C. EFFECT OF WELDING SPEED	48

D. WELD POOL SURFACE FLOWS AND FEATURES	52
1. Weld Pool Depression and Rise	59
2. Weld Pool Surface Flows	60
V. CONCLUSIONS	67
LIST OF REFERENCES	69
INITIAL DISTRIBUTION LIST	72

LIST OF TABLES

TABLE I.	SELECTED COMPUTATIONAL STUDIES OF WELD POOL CONVECTION.	2
TABLE II.	EXPERIMENTAL STUDIES OF WELD POOL FLUID FLOW AND HEAT TRANSFER.	6
TABLE III.	SPECTRAL CHEMICAL ANALYSIS OF HY-80 (REPORTED AS WT.%)	12
TABLE IVA.	EFFICIENCY LISTED AT INDICATED POWER SETTING FOR BLUNT (90°) ELECTRODE TIP AND 3 MM ARC.	22
TABLE IVB.	EFFICIENCY LISTED AT INDICATED POWER SETTING FOR ELECTRODE TIP ANGLES OF 45° AND 4 MM ARC.	22
TABLE IVC.	EFFICIENCY LISTED AT INDICATED POWER SETTING AND ARC LENGTH FOR ELECTRODE TIP ANGLES OF 45°	22
TABLE VA.	RELATION BETWEEN DIRECTION AND ORIENTATION OF GROUND OFF-TAKE AND VISIBLE SURFACE FLOWS. <u>ALL FLOWS OBSERVED WERE IN THE CLOCKWISE DIRECTION.</u>	25
TABLE VB.	RELATION BETWEEN DIRECTION AND ORIENTATION OF GROUND OFF-TAKE AND VISIBLE SURFACE FLOWS.	25
TABLE VI.	COMPREHENSIVE LISTING OF STATIONARY ARC EXPERIMENTS	42
TABLE VIIA.	SUMMARY OF WELDING PARAMETERS AND WELD POOL MEASUREMENTS	44
TABLE VIIB.	SUMMARY OF WELDING PARAMETERS AND WELD POOL MEASUREMENTS	45
TABLE VIII.	CALCULATED EFFICIENCIES.	47
TABLE IX.	CALCULATED WELD POOL DIMENSIONS.	59
TABLE X.	REVIEW OF SELECTED REPORTED SPEEDS.	63

LIST OF FIGURES

Figure 1.	Laser-Augmented Welding Vision System. . .	14
Figure 2.	Laser Vision System Camera Mounted on Tripod.	15
Figure 3.	Weld Pool Cross Section 251V, 13.2A, 4mm Arc, 45° Electrode Tip Angle. Scale 15.75 Marks Per Centimeter. Enlargement x5.7. .	20
Figure 4.	Clockwise Rotation of Stationary Weld Pool. 200A, 14.0v, 4 mm Arc Length, 20° Electrode Tip Angle, Weld Pool Diameter 14.2 mm. Enlargement x7.7.	23
Figure 5.	Counter Clockwise Rotation of Stationary Weld Pool. 200A, 0.2v, 4 mm Arc Length, 45° Electrode Tip Angle, Weld Pool Diameter 10.0 mm. Enlargement x5.7. . . .	24
Figure 6.	Weld Pool Growth With Time. 20° Electrode Tip Angle, 4 mm Arc Length.	27
Figure 7.	Weld Pool Growth With Time. Expansion of 0-5 Second Interval From Figure 6. 20° Electrode Tip Angle, 4 mm Arc Length. . .	28
Figure 8.	Weld Pool Growth With Time. Expansion of 0-1 Second Interval From Figure 6. 20° Electrode Tip Angle, 4 mm Arc Length. . .	29
Figure 9.	Weld Pool Growth With Time. 45° Electrode Tip Angle, 3 mm Arc Length.	30
Figure 10.	Weld Pool Growth With Time. 90° Electrode Tip Angle. 5 mm Arc Length.	31
Figure 11.	Effect of Changes in Arc Length.	33
Figure 12.	Electrode Tip Angles.	34
Figure 13.	Effect of Changes in Electrode Tip Angle.	35

Figure 14.	Weld Pool Rise, 1.2 mm, 300A, 14.8v, Arc Length 3mm, 45° Electrode Tip Angle. Weld Pool Diameter 14.1 mm. Enlargement x5.0.	37
Figure 15.	Weld Pool Rise for Various Power Levels and Electrode Tip Angle.	38
Figure 16.	Weld Pool Rise for Various Power Levels and Arc Lengths.	39
Figure 17.	Weld Pool Oscillations, 200A, 14.0v, 4mm Arc Length, 20° Electrode Tip Angle. Weld Pool Oscillates From Right (a) to Left (b) Back to Right (c). Enlargement x5.0.	41
Figure 18	Coordinate System.. . . .	46
Figure 19.	Effect of Input Power. Larger Input Powers Produce Larger Welds.	49
Figure 20.	Effect of Input Power. Larger Input Powers Produce Larger Welds.	50
Figure 21.	Effect of Input Power. Larger Input Powers Produce Larger Welds.	51
Figure 22.	Effect of Welding Speed. Faster Moving Arc Welds Produce Smaller Weld Pools. . .	53
Figure 23.	Effect of Welding Speed. Faster Moving Arc Welds Produce Smaller Weld Pools. . .	54
Figure 24.	Effect of Welding Speed. Faster Moving Arc Welds Produce Smaller Weld Pools. . .	55
Figure 25.	Effect of Welding Speed. Faster Moving Arc Welds Produce Smaller Weld Pools. . .	56
Figure 26.	Effect of Speed on % of Weld Pool Leading Arc. Faster Moving Arc Welds Have Small % of Weld Pool Leading Arc.	57
Figure 27.	Effect of Speed on % of Weld Pool Leading Arc. Faster Moving Arc Welds have Small % of Weld Pool Leading Arc.	58
Figure 28.	Weld Pool Depression. 250A, 14.3 v, Welding Speed .85 mm/sec. Actual Weld	

	Pool Width of 11.1 mm. Enlargement x4.0.	61
Figure 29.	Solidified Weld Bead Showing 0.5 mm Rise at Center of Weld. 250A, 14.2 v, Welding Speed 4.17 mm/sec. Enlargement x3.2 . . .	62
Figure 30.	Weld Pool Flow. Time + 0 Seconds, 250 A, 14,2 v, Welding Speed 2.27 mm/sec. Enlargement x5.5.	64
Figure 31.	Weld Pool Flow. Time + .02 Seconds, 250 A, 14.2 v, Welding Speed 2.27 mm/sec. Enlargement x5.5.	65
Figure 32.	Weld Pool Flow. Time + .04 Seconds, 250 A, 14.2 v, Welding Speed 2.27 mm/sec. Enlargement x5.5.	66

I. INTRODUCTION

A. SELECTED HISTORY OF NUMERICAL INVESTIGATIONS

Limitations in the speed and inconsistent quality control of manual Gas Tungsten Arc Welding (GTAW) process have resulted in the need for automatic welding control systems. For nearly two decades, scientists have sought to develop an automatic system. While partial automation has been successful for certain applications, no system has been developed so far which detects and corrects for variation in numerous welding parameters such as material composition, shape of the electrode, variations in the flow of shielding gas, arc blow and oxide patches. These are a few of the weld quality parameters that a highly skilled operator monitors and are necessary ingredients of a truly automatic system.

In recent years, progress towards a truly automatic system has been made using computer simulations of the welding process. These simulations are based on mathematical models of heat and fluid flows in the welding arc, weld pool, and the surrounding heat affected zone. Verification of such models is a difficult task due to the transient nature of welding and the inherent problems with ultra high temperature and high luminosity measurements. A summary of some of the recent computational studies is provided in Table I.

**TABLE I. SELECTED COMPUTATIONAL STUDIES OF
WELD POOL CONVECTION.**

INVESTIGATOR(S)	REFERENCE	REMARKS
1. Oreper and Szekely	<i>J. Fluid Mech</i> (1984)	Heat and Fluid-flow phenomena in weld pools are modeled for the TIG (tungsten-inert-gas) welding system. Formulation included electromagnetic, buoyancy and surface tension forces. Inward or outward surface tension driven flows may be altered by changing process chemistry.
2. Kou and Wang	<i>Met. Trans A</i> (1986)	Computer simulation of convection in moving arc weld pools with same driving forces as in [1]. Model assumes flat weld pool surface and predicts radially outward flow with partial penetration and inward flow with full penetration. Surface tension gradients cause flow direction to change.
3. Saedi and Unkel	<i>J. of Dyn. Sys. Measurement and Control</i> (1989)	Thermal-fluid modeling for weld pool geometry dynamics was conducted using an assumption of a single circulation patterns (outward or inward radial) inside the pool with the E-M forces dominating.
4. Zacharia et al.	<i>Met. Trans. 13</i> (1989)	Three-dimensional transient model for arc welding process was developed. Weld pool surface is assumed to be deformable and formation of weld pool crown is acknowledged. Stationary and moving arc weld pool exhibit radially outward flows.
5. Kim and Na	<i>J. of Eng Manufacture</i> (1989)	A study on heat and mass flow in stationary gas tungsten arc welding using the numerical mapping method. Model was developed using three driving forces considered in [1]. With the addition of the effect of aerodynamic drag force due to the impinging plasma jet. Combined effect caused double loop circulation.
6. Zacharia et al.	<i>Welding Research Supplement</i> (1989)	Theoretical analysis of weld pool development during GTA welding was conducted using the same three driving forces as in [1] with surface tension being a function of temperature and sulfur content. Surface tension gradient driven flow dominates the fluid flow and the development of the weld pool. Outward or inward flows were predicted depending on sulfur content.
7. Ule et al.	<i>Met. Trans 21B</i> (1990)	Three-Dimensional transient heat transfer computations. Model assumes distributed heat source and produces only temperature contour lines for fusion zone prediction. No surface flow information.

One of the earliest approaches to the modeling of weld pool convection is that by Oreper and Szekely [Ref. 1]. Their model was based on three separate driving forces for the TIG (tungsten-inert-gas) process: the electromagnetic force which is caused by the interaction between the divergent current path in the weld pool and the magnetic field it generates, the buoyancy force which is caused by the temperature gradient within the weld pool in the presence of the gravity field and the surface tension gradients caused by temperature gradients along the weld pool free surface. The latter can be altered by the presence of surface active agents in the weld pool [Ref. 1:p. 71].

Using a similar approach Kou and Wang [Ref. 2] modeled weld pool convection using the same three driving forces as Oreper and Szekely. Both models assume a flat weld pool surface, and claim to be applicable for currents at or below 200A. Both models indicate fluid flow on the surface away from or towards the center of the weld pool, depending upon the behavior of surface tension with the temperature, during moving arc welding. [Ref. 3]

Another recent attempt at modeling was by Saedi and Unkel [Ref. 4]. Their approach was limited to stationary arc cases with deep parabolic pool geometry. In addition to the electromagnetic, surface tension, and buoyancy forces, they considered the pressure and shearing force on the surface of the weld pool due to the plasma jet momentum as a possible

physical mechanism responsible for convection inside the weld pool. Their model assumed that electromagnetic forces dominate the circulation pattern inside the weld pool but that a top region exists where surface tension forces dominate, creating the same type of outward and inward surface flows which the first two studies mentioned. The model that Saedi and Unkel developed was too long to be used in real time due to the computational time of the conduction solution; however, it closely followed experimental observations of top width and penetration.

A recent study by Zacharia et al. [Ref. 5] begins by attempting to simulate the entire welding process. To analyze the entire process, they state the need to take into account the following:

- heat transfer from the arc to the metal surface.
- coupled conduction and convective heat transfer.
- fluid flow in the weld pool.
- phase transformation (melting and solidification) at the solid/liquid interface.
- fusion zone geometry.
- convection and radiation heat transfer between the specimen and the atmosphere.
- realistic weld geometry.
- accurate physical properties for the metal.

Their model indicates that surface tension is the predominant force that controls convection in stationary arc welding

causing an outward fluid flow from the weld pool center. This results since pure metals surface tension is highest at the cooler edges of the weld pool which forces the fluid away from the center of the weld pool. A weld pool crown develops from accumulation of molten metal at fusion zone interface caused by faster moving liquid on the surface than in the bulk of the weld pool. The outward predicted flow is also believed to cause a depression of the metal surface at the center of the pool. [Ref. 5:p. 654]

Two other studies, one by Kim and Na [Ref. 6], the other by Zacharia et al. [Ref. 7], also predict inward or outward radial surface flows which depend mainly on surface tension. Both are summarized in Table I.

A report by Ule et al. [Ref. 8] looks at three-dimensional transient temperature variations during autogenous gas tungsten arc welding. The model assumes a distributed heat input source and provides the capability of computationally predicting the effects of varying welding parameters. This would allow a real time weld quality monitoring or control system based on temperature sensing.

B. SELECTED HISTORY OF EXPERIMENTAL INVESTIGATIONS

Experimental studies on weld pool motion, summarized in Table II, not only enable the verification of computer models but they also give insight into three related issues associated with welding quality. First, weld pool motion or

**TABLE II. EXPERIMENTAL STUDIES OF WELD POOL FLUID FLOW
AND HEAT TRANSFER.**

INVESTIGATOR(S)	REFERENCE	REMARKS
1. Woods and Milner	<i>Welding J.</i> (1971)	Studying motion in the weld pool in arc welding by producing visualization of metal pools that suggest fluid flow. Motion is primarily caused by the Lorentz force and is circular in nature. Asymmetric current path gives rise to pure rotation.
2. Metcalfe and Quigley	<i>Welding J.</i> (1977)	Studying arc and pool instability in GTA welding by identifying weld pool surface films that influence anode spot behavior. Visualization was achieved using microscope with camera and filter attachments. Floating surface scum revealed motion "around" the metal.
3. Bolstad	<i>EG&G Report</i> (1987)	Presenting a new electronic imaging technique for welding.
4. Kraus	<i>Welding J.</i> (1989)	Experimental measurements of stationary GTA weld pool surface temperatures infer weld pool circulation patterns. Circulation patterns as related to surface temperature profiles may differ from run to run due to variation in any welding parameters.
5. Malinowski-Brodnicka et al.	<i>Welding J.</i> (1990)	Studying effects of electromagnetic stirring on GTA welds in austenitic stainless steel. Changes in shape and solidification structure of welds observed. Application of an external magnetic field causes rotation of arc and annular flow of the liquid metal in the weld pool.
6. Voelkel and Mazumder	<i>App Optics</i> (1990)	Presenting a modification to the new electronic imaging technique for welding as listed in [3].

stirring facilitates heat transfer in the weld pool thereby effecting weld pool dimensions. Second, stirring determines the overall homogeneity of the weld bead. Lastly, stirring increases the opportunities for metal, flux, and filler constituents to react in the weld pool, effecting strength and weld quality. One such study of weld pool motion was by Woods and Milner [Ref. 9]. By using a rapid quench process, stirring action by arc welding was made observable. Research on bismuth-tin metals with indium added for trace material showed circular motion around the weld pool center [Ref. 9:pp. 16677-s]. Furthermore, pure rotation was observed under given conditions. These results are in striking contrast to the mathematical models mentioned earlier.

Experiments on the pattern of fluid flow by Woods and Milner also showed a relation to position and orientation of the ground for the welded material. In addition, even when using reverse polarity, circular motion was still observable. Woods and Milner's approach to weld pool motion led them to the conclusion that the circular motion was caused by electromagnetic and plasma jet momentum forces.

Metcalf and Quigley [Ref. 10], while studying arc and pool instability in GTA welding, produced cine-photography of the arc and weld pool surface. The film was run at 250 frames per second and neutral density filters were used to reduce light intensity without altering the color balance. Metcalf and Quigley report observing large lumps of slag floating

"around" on the surface of the weld pool. No information on the direction was noted. In addition to slag they also reported a thin dark layer of scum which is easily moved by the surface currents on the weld pool and a more tenacious form of scum adhering to the weld pool sides. Their analysis of the scum and slag indicate that the material contained higher than expected levels of aluminum and titanium.

Bolstad [Ref. 11] presented a new electronic imaging technique for the welding process. The purpose of his report was to show that the weld pool surface feature can be clearly observed by shuttering and filtering. This imaging technique is described in Chapter II, and is used in the present study.

A recent experimental study on stationary weld pool by Kraus [Ref. 12] related surface temperatures to convective circulation patterns present. An optical spectral radiometric/laser reflectance method was used to produce high-resolution surface temperature maps of stationary GTA molten weld pools using SS 304, SS 316L, and 8630 steel. Measurements of the weld pool dome to account for non-flat weld pool surfaces were reported. A range of heats were used to study the effects of minor alloying elements on the weld pool surface temperatures. Speculations on the surface tension-induced surface circulation patterns were also provided based on the surface temperature measurements.

A study by Malinowski-Brodnicka et al. [Ref. 13] indicates that application of an external axial magnetic field during

welding has a significant influence on the shape and solidification of the weld. Using bead on plate welds with a steady magnetic field, asymmetric weld beads were formed; asymmetry increasing with increasing field strength. Applying an alternating magnetic field produced symmetric weld bead of regular and predictable shape. Malinowski-Brodnicka et al., stated that the weld bead shape and weld metal structure are a result of arc rotation and turbulent flow in the liquid metal of the weld pool.

Voelkel and Mazumder [Ref. 14] discuss visualization of a laser melt pool using a method similar to the system presented in Bolstad's report [Ref. 11] which is detailed in Chapter II. An illumination technique using both focused and diffused light is used to deal with the high contrast, obscuring plasma, and specular surface. As in the Bolstad report [Ref. 11] the article describes the experimental technique and does not cover details of surface flow patterns.

C. PRESENT EXPERIMENTAL INVESTIGATION

In the present study, the electronic imaging technique [Ref. 11] for arc welding was used. This technique allowed direct viewing of the weld pool with minimum interference from the extremely bright arc of the welding plasma. The weld pool was seeded with alumina particles whose motion was used for inferring the flow pattern on the free surface of the pool. Effects of welding power, electrode tip shape, and arc length

on weld pool free surface flows were studied. Both stationary and moving GTA processes were examined. [Ref. 11]

II. EXPERIMENTAL SET-UP AND PROCEDURE

A. GAS TUNGSTEN ARC WELDING APPARATUS

A Miller DC Welding Power Source, Model SR600/SCMIA with electroslope 3 was used in all stationary and moving arc welds. Direct current straight polarity, also referred to as direct current electrode negative, was utilized which is also recommended by Stinchcomb [Ref. 15] for welding of mild steel. To improve the accuracy of current and voltage readings a Miller Dig-Meter Model 600 volt and 900 amp meter was used to directly measure current and voltage. Also recommended by Stinchcomb and utilized in all the data collection were 2% Thoriated tungsten electrodes, number 6 cup, and argon gas. Argon shielding gas flow rates of 118-157 mili-liters per second (15 to 20 cubic feet per hour) were used. Three-dimensional positioning of the torch was facilitated by motor controlled traverses. [Ref. 16]

B. MATERIAL CHARACTERISTICS

HY-80 was selected as the welding material due to its vast use in naval applications. HY-80 is a high yield, extremely weldable, quenched and tempered steel. This material responds well to dynamic loading at low temperatures, consequently it is the preferred material for submarines and other vessels.

Twelve-by-seven-inch, one-inch thick HY-80 plates were welded with 18 spot welds or six moving arc welds. The liquidus and solidus temperatures are 1516°C (2760°F) and 1468°C (2675°F) respectively. [Ref. 17]

Table III below shows the results of spectral chemical analysis of three representative HY-80 plates utilized.

**TABLE III. SPECTRAL CHEMICAL ANALYSIS OF HY-80
(REPORTED AS WT.%)**

		Sample 1	Sample 2	Sample 3
Aluminum	(Al)	0.03	0.03	0.02
Carbon	(C)	0.14	0.16	0.16
Chromium	(Cr)	1.49	1.46	1.48
Columbium	(Cb)	<0.005	<0.005	<0.005
Copper	(Cu)	0.10	0.04	0.03
Manganese	(Mn)	0.23	0.30	0.30
Molybdenum	(Mo)	0.37	0.36	0.38
Nickel	(Ni)	2.79	2.52	2.52
Nitrogen	(n)	0.015	0.009	0.009
Phosphorus	(P)	0.010	0.007	0.007
Silicon	(Si)	0.25	0.25	0.25
Sulfur	(S)	<0.005	0.018	0.017
Tin	(Sn)	0.009	<0.005	<0.005
Titanium	(Ti)	<0.005	<0.005	<0.005
Vanadium	(V)	<0.005	<0.005	<0.005

C. WELD POOL VISUALIZATION SYSTEM

A laser-augmented welding visor system was utilized and was set up as in Figure 1. This electronic imaging technique was specifically developed for uses where electric arc, plasmas, flames and self luminosity of the material would

normally interfere with the imaging process [Ref. 11]. Laser light more intense than welding arc is directed towards the welding site and strobed in unison with a conventional night vision image-intensifier tube. The results are clearer than any normal video, and are filmed using a solid-state video camera. The video may then be viewed directly on a TV monitor and recorded on a VCR. [Ref. 18] [Ref. 11]

1. Laser

The light source is a Laser Photonics PRA/Model UV12 Pulsed Nitrogen Laser. This laser required an external vacuum and external supply of nitrogen. The laser was operated at 60 pulses per second requiring a supply of 315 mili-liter per second (40 standard cubic feet per hour) of nitrogen and a vacuum pump capable of maintaining 60 torr. [Ref. 19]

2. Vision System

The camera unit and system controller is a Control Vision Inc. Model PN-232 Laser-Augmented Welding Vision system. The camera unit, seen in Figure 2, may be mounted on any standard photographic tripod and is placed 15 to 31 centimeters (6 to 12 inches) away from the welding site. The optical head included the objective optics and optical filter with the straight end-viewing configuration. This configuration allows the operator to direct the camera at any area of interest using any angle obtainable. Focusing area of the camera is between 1-16 cm² where the upper end is limited

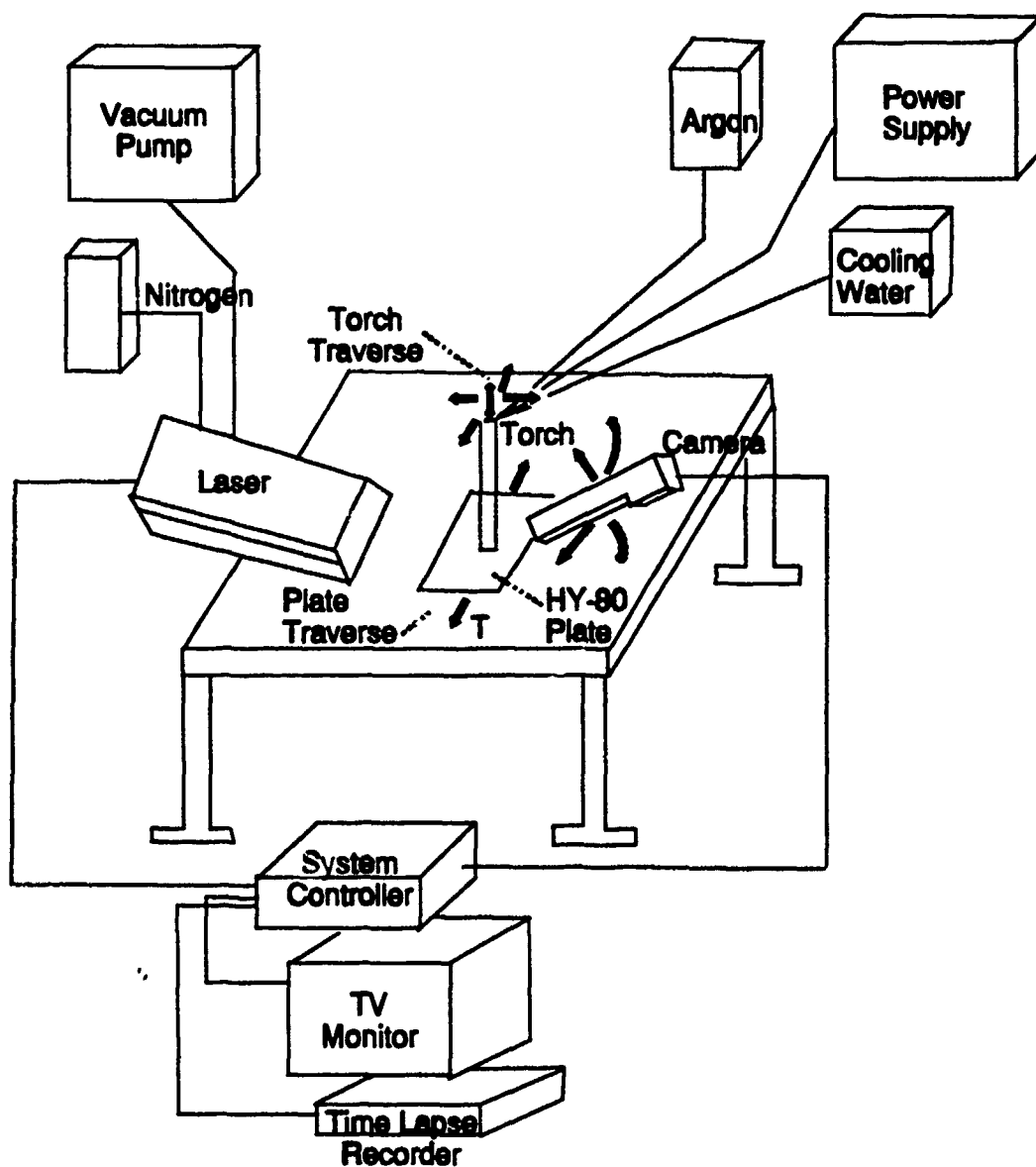


Figure 1. Laser-Augmented Welding Vision System.

by the illumination pattern size and intensity of the laser. The system controller fires the laser and shutter on the camera unit in unison. Because of an electronic delay associated with firing of the laser and the shutter a manual



Figure 2. Laser Vision System Camera Mounted on Tripod.

shutter delay setting is required on the controller. A shutter delay of $0.64 \mu\text{s}$ was utilized and provided the best video. A camera sensitivity adjustment is possible and was made when striking the arc. The camera sensitivity was placed at the lowest possible setting when striking the arc and then raised to the desired level when in normal operation. [Ref. 18]

3. Monitor and Recording

A Panasonic video monitor Model TR-196M was used in high impedance mode and provided high resolution viewing of the weld pool in black and white on a 19-inch screen. Video was recorded on a VHS Panasonic Time Lapse Recorder Model A6-

6720-P. The recorder provides 400 lines of horizontal resolution and provides an extremely fine slow motion playback allowing each of the 60 frames per second to be viewed individually at slow speed in sequence or in reverse order. Hard copy photographs of individual frames were obtained by slow speed manual professional photography of the 19-inch high resolution monitor while pausing at the desired frame.

D. EXPERIMENTAL PROCEDURE

To provide a basis for comparison with computations, experiments were carried out for stationary weld pools and for bead on plate moving arcs. The experiments concentrated on the recording of surface weld pool development and surface flows.

The experimental procedure consisted of the following steps:

1. Sample Preparation

In all experimental runs, HY-80 plates were cleaned of oil, moisture, and contaminants by passing oxyfuel torch over the steel and then wire brushing all surfaces to be welded. Sectioning and numbering preceded the coating of each surface with fine alumina particles. Plates were positioned for stationary arc welding or placed in motion by a lower table traverse.

2. Vision System Preparation

Once manual placement of laser and camera components were complete, synchronization at 60 frames per second was

achieved using the vision system camera controller. Focusing of the image on the monitor was completed prior to striking the arc and the time lapse recorder was placed in the continuous record mode using VHS tapes.

3. Welding Equipment

Argon flow, cooling water flow, arc length, and current were adjusted and then the arc was struck. Immediate fine current adjustments were made to set current at desired level.

III. STATIONARY ARC EXPERIMENTS

This chapter will cover stationary bead on plate welds. Durations of experimental welds were on the order of 30-50 seconds. Stationary experiments included studying welding efficiency, ground effects, and weld pool development. Reasonable approximations of welding efficiency can be used in numerical models to predict weld pool size characteristics which in turn can be indicative of weld pool convection flow patterns. Ground effects experiments were conducted in order to determine if the placement and orientation of ground effected surface flow patterns. Weld pool development with time was examined with emphasis on effects of input power, arc length and electrode tip angle. For all experiments video images of weld pool were produced in order to report on weld pool sizes and surface flow patterns. A comprehensive listing of stationary arc experiments can be found in Table VI at the end of this chapter.

A. WELDING EFFICIENCY

Fusion welding processes are extremely difficult to model accurately due to the widely varying parameters under which the process takes place. The welding efficiency is a parameter which needs to be provided in numerical simulations of the process. Published welding efficiencies vary widely (20%-90%)

due to deviations in welding or machine parameters. One objective of the present study was to determine the effect of several common welding variables on the efficiency of the GTAW process.

Efficiency (η) of the welding process can be defined as follows:

$$\eta = \frac{\text{Rate of energy transferred to the workpiece}}{\text{Rate of energy generated by the heat source}} \quad (1)$$

The denominator in Equation (1) is the product of input voltage and current. The quantity in the numerator can be estimated using Rosenthal's [Ref. 20] three-dimensional heat flow solution. Setting velocity equal to zero gives;

$$q = 2\pi Kr(T_m - T_o) \quad (2)$$

Simplifying Equations (1) and (2), efficiency can be reduced as follows:

$$\eta = \frac{2\pi Kr_o(T_m - T_o)}{EI} \quad (3)$$

where

q	=	energy transferred to the workpiece
K	=	rate of thermal conductivity of the workpiece
r _o	=	distance from center of weld pool to fusion zone
T _m	=	temperature at fusion (solidus temperature)
T _o	=	ambient temperature of material far away from the torch
I	=	current
E	=	voltage

In Equation (3), r_o was determined by welding on the sample, cutting the bead in order to reveal the center cross-section, preparing the samples (see [Ref. 8]) and photographing the

prepared surfaces for measurements as seen in Figure 3 and provided measurements with an uncertainty of 0.2mm. Efficiencies determined using Equation (3) are listed in Tables IVA through IVC. The range of efficiency values listed is 55 to 77 percent. Giedt et al. [Ref. 22] report published values from 21% to 80% and experimentally obtain a value around 80% using a gradient layer type calorimeter when welding 304L stainless steel.

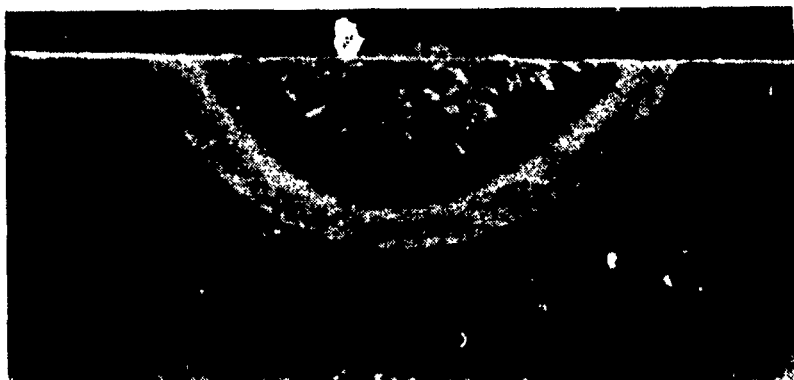


Figure 3. Weld Pool Cross Section 251v, 13.2A, 4mm Arc, 45° Electrode Tip Angle. Scale 15.75 Marks Per Centimeter. Enlargement x5.7.

As seen in Tables IVA and IVB, an increase of input power decreased efficiency. Also arc length does not appear to significantly effect efficiency as seen in Table IVc. While conducting moving arc experiments, Niles and Jackson [Ref. 23] also observed both a decreasing efficiency with increasing power input and a negligible effect of electrode angle on

efficiency. It is clear that arc efficiency depends on welding parameters such as input power but its calculation also depends on the theoretical model utilized. Giedt [Ref. 24] showed that higher efficiency values are calculated with realistic conduction models. These models account for surface convective losses, use distributed heat sources and often account for the latent heat of fusion. While the measurements reported in Tables IVA-IVC do not account for these effects, Table VI reports the raw data from which such corrected values can be computed.

B. GROUNDING EFFECTS

In the electrode negative GTA welding configuration the arc impinges vertically onto the weld pool, the electrons then flow through the weld pool and to the ground off-take point. Position and orientation of ground off-take were varied after each bead on plate. Welding positions varied from center of the plate to a distance of two inches from the edge. When welding on the center of the plate, rapid clockwise weld pool surface flows were visible. Varying position and orientation of ground off-take did not effect the observed clockwise flow when welding on the center of the plate. Table VA shows the various positions and orientations of ground and the resulting flow direction observed. Figure 4 shows examples of these clockwise surface flow patterns.

TABLE IVA. EFFICIENCY LISTED AT INDICATED POWER SETTING FOR BLUNT (90°) ELECTRODE TIP AND 3 MM ARC.

AMPS	VOLTS	POWER (WATTS)	η (%)
303	14.3	4333	55
251	12.2	3062	61
200	11.1	2220	67

TABLE IVB. EFFICIENCY LISTED AT INDICATED POWER SETTING FOR ELECTRODE TIP ANGLE OF 45° AND 4 MM ARC

AMPS	VOLTS	POWER (WATTS)	η (%)
300	14.8	4440	56
251	13.2	3313	59
202	13.2	2666	77

TABLE IVC. EFFICIENCY LISTED AT INDICATED POWER SETTING AND ARC LENGTH FOR ELECTRODE TIP ANGLE OF 45°

ARC LENGTH	AMPS	VOLTS	POWER (WATTS)	η (%)
3	300	12.9	3870	63
4	300	14.8	4440	56
5	300	16.2	4860	65

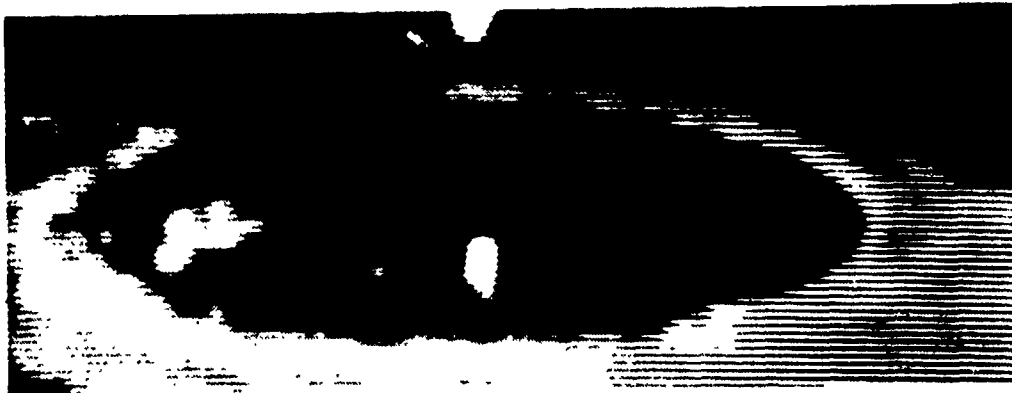
The results of ground effects when welding on the center of the plate are in sharp contrast to ground effects when welding near the plate edge (within two inches). Table VB shows positions and orientation of ground and the flow direction observed for the latter conditions. Flows varied from rapid clockwise to slow counter-clockwise as position and orientation of ground changed. An example of clear counter-clockwise rotation is seen in Figure 5. Woods and Milner [Ref. 9:pp. 1695] conducted experiments on the pattern of fluid



a. Time + 0 Seconds



b. Time + 0.2 Seconds



c. Time + 0.4 Seconds

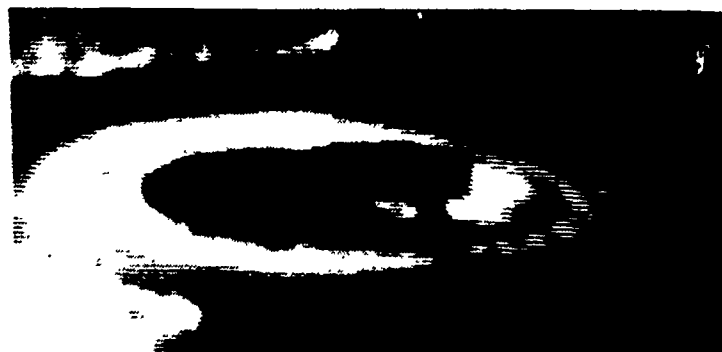
Figure 4. Clockwise Rotation of Stationary Weld Pool. 200A, 14.0v, 4 mm Arc Length, 20° Electrode Tip Angle, Weld Pool Diameter 14.2 mm. Enlargement x7.7.



a. Time 0.0 Seconds



b. Time +0.2 Seconds



c. Time +0.4 Seconds

Figure 5. Counter Clockwise Rotation of Stationary Weld Pool. 200A, 0.2v, 4 mm Arc Length, 45° Electrode Tip Angle, Weld Pool Diameter 10.0 mm. Enlargement x5.7.

TABLE VA. RELATION BETWEEN DIRECTION AND ORIENTATION OF GROUND OFF-TAKE AND VISIBLE SURFACE FLOWS. ALL FLOWS OBSERVED WERE IN THE CLOCKWISE DIRECTION.

Bead on Plate at Center of Plate

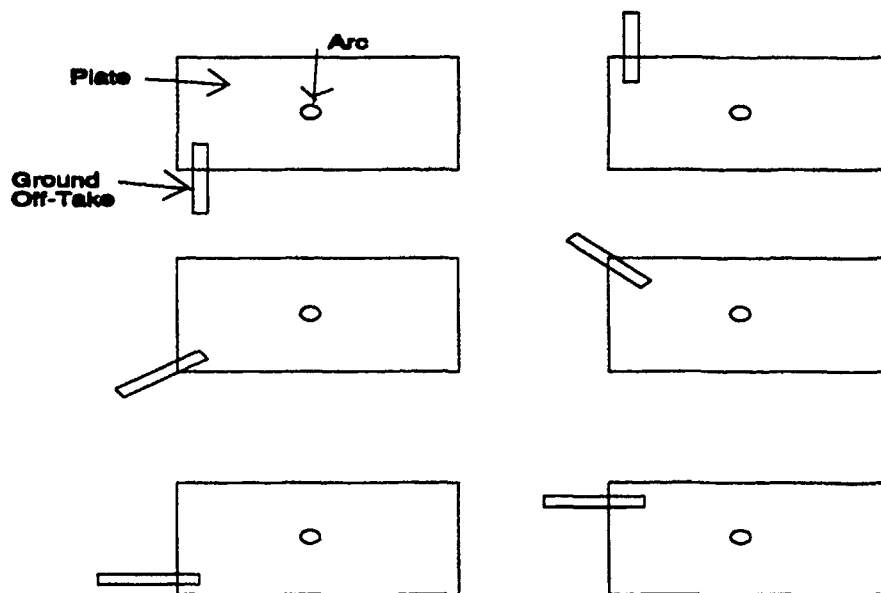
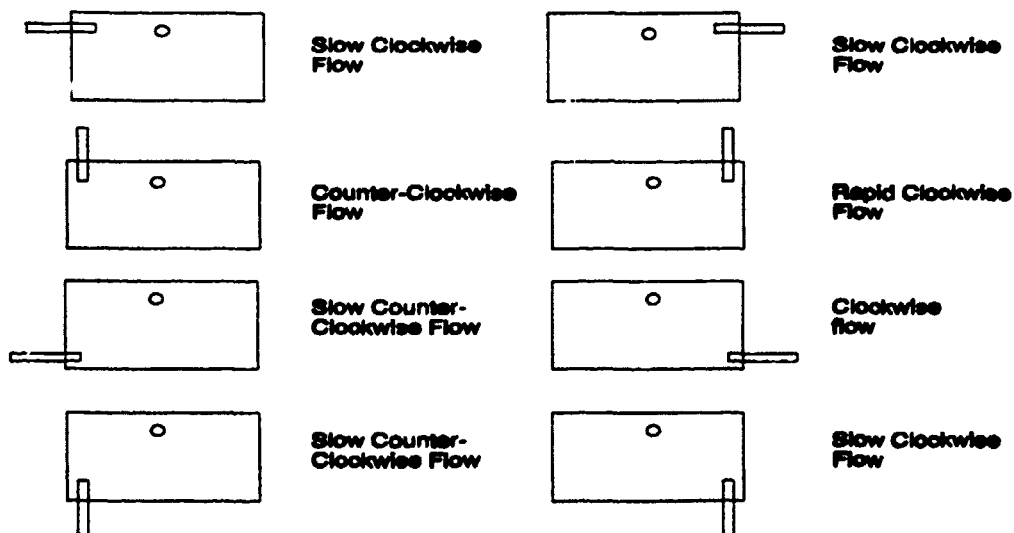


TABLE VB. RELATION BETWEEN DIRECTION AND ORIENTATION OF GROUND OFF-TAKE AND VISIBLE SURFACE FLOWS.

Bead on Plate Two Inches From Edge of Plate



flows in relation to the direction of the current off-take connection. Their experiments simulated bead on plates at or below 200 Amps and they were able to produce both clockwise and counter-clockwise flows. Numerical models discussed in Chapter I do not predict circular flows around the weld pool. This is in direct contrast to the present observations.

C. WELD POOL DEVELOPMENT

Many of the stationary welding experiments were oriented towards the study of weld pool development. Weld pool growth for bead on plate was analyzed from the arc being struck to complete weld pool development (0-45 seconds). Figures 6-10 show weld pool development as a function of time and highlight the effects of input power, arc length and electrode tip angle. As noted in Chapter II, 60 frames per second were recorded. Each individual frame was then counted and studied for such items as weld pool size, surface flow patterns, and free surface rise.

1. Effect of Input Power Changes

There are two clear trends among all the experiments regarding input power. They are as follows: first, weld pool diameter increases as input power increases, and second, lower power weld pools generally reach steady state diameter before higher power weld pools. These two observations can be seen clearly in Figures 6-8 and are independent of arc length and electrode tip angle shown in Figures 9-10. Rosenthal's [Ref.

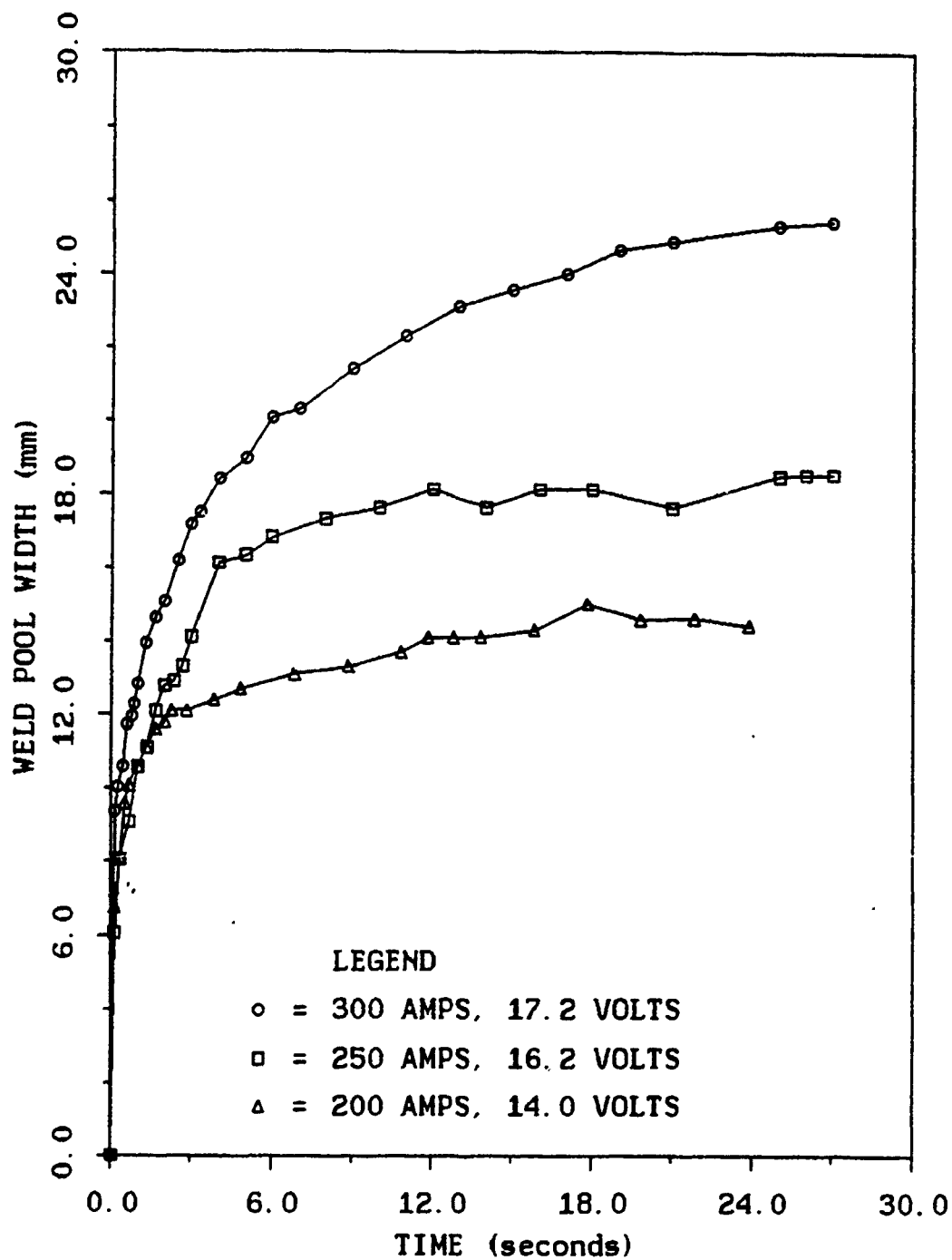


Figure 6. Weld Pool Growth With Time. 20° Electrode Tip Angle, 4 mm Arc Length.

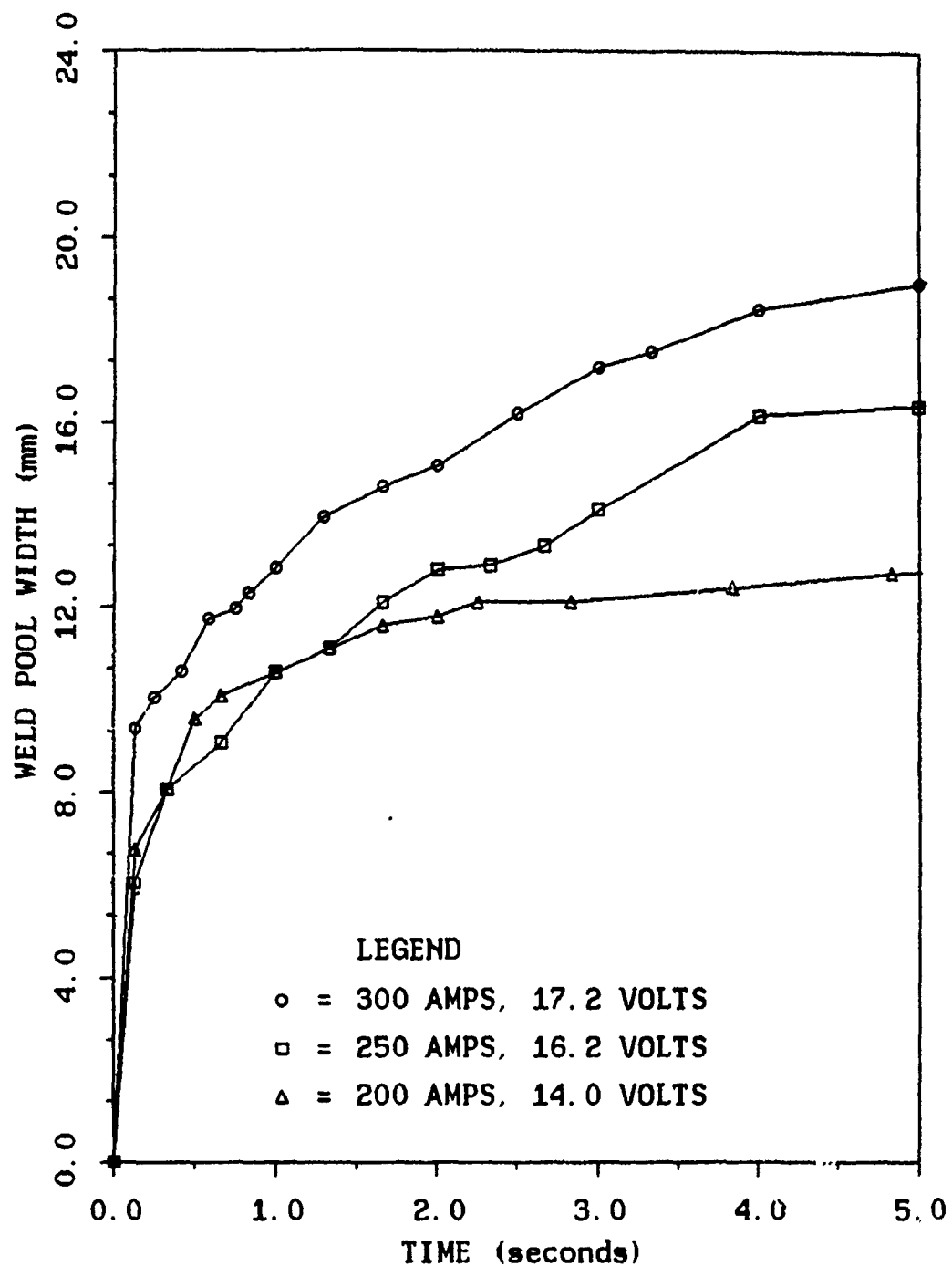


Figure 7. Weld Pool Growth With Time. Expansion of 0-5 Second Interval From Figure 6. 20° Electrode Tip Angle, 4 mm Arc Length.

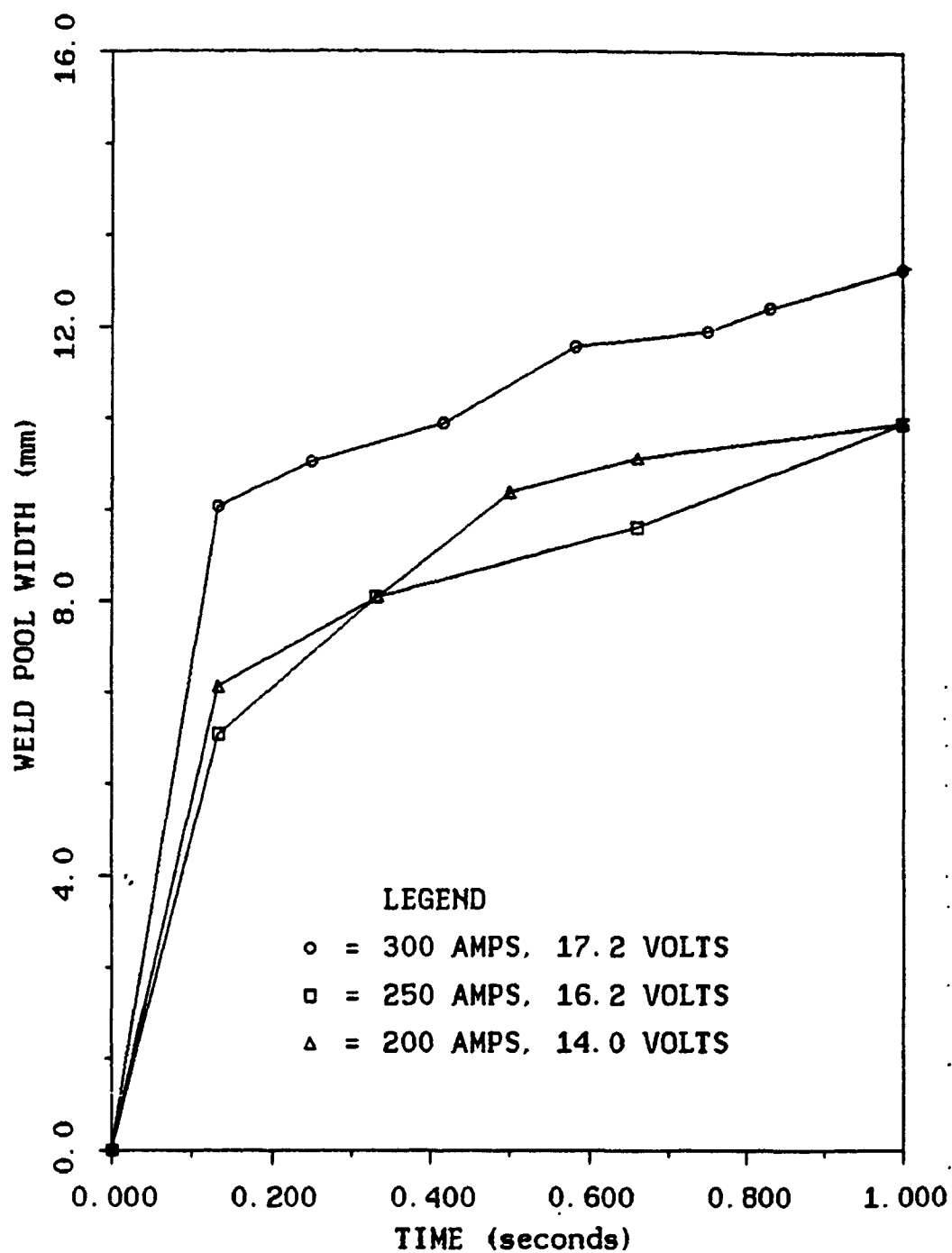


Figure 8. Weld Pool Growth With Time. Expansion of 0-1 Second Interval From Figure 6. 20° Electrode Tip Angle, 4 mm Arc Length.

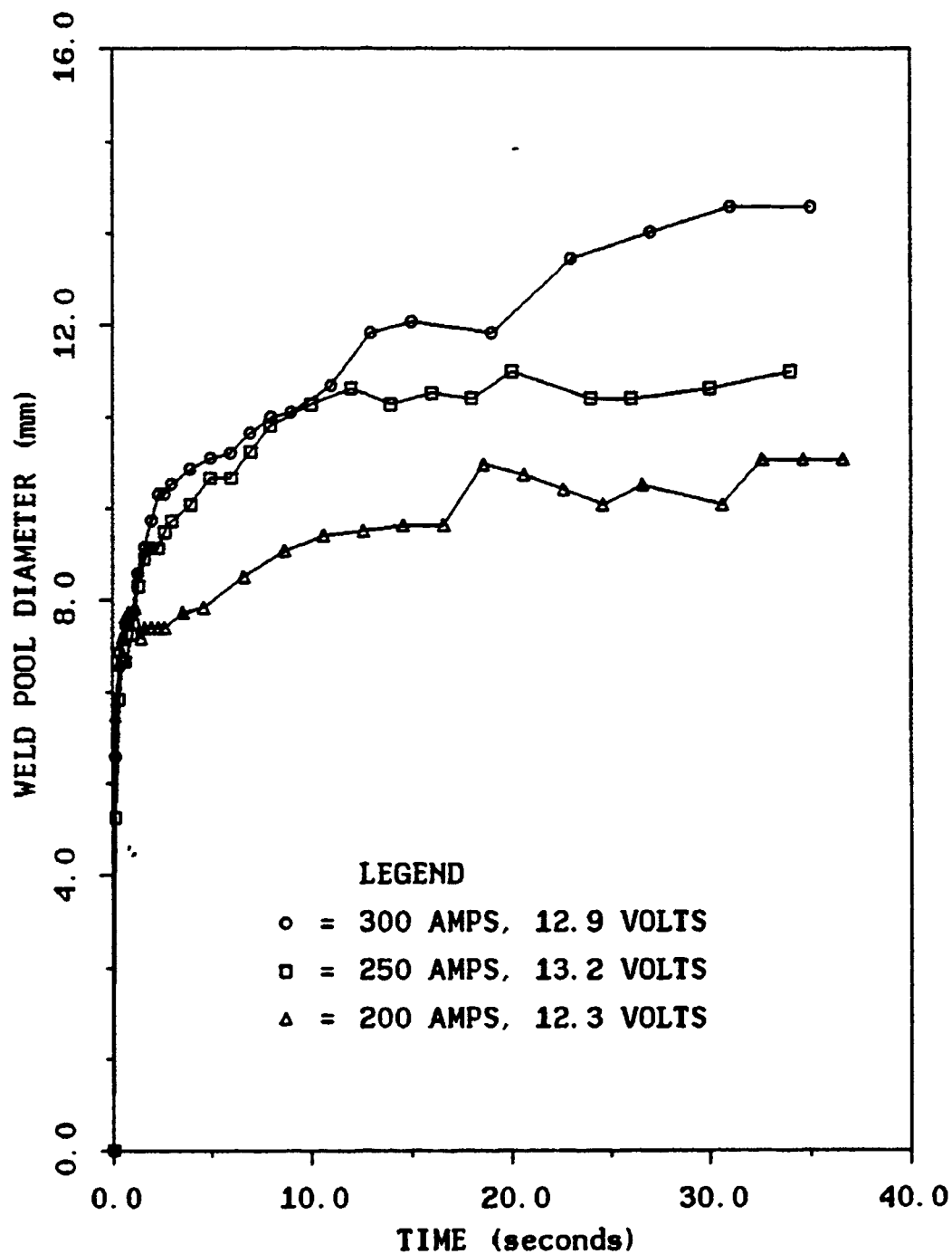


Figure 9. Weld Pool Growth With Time. 45° Electrode Tip Angle, 3 mm Arc Length.

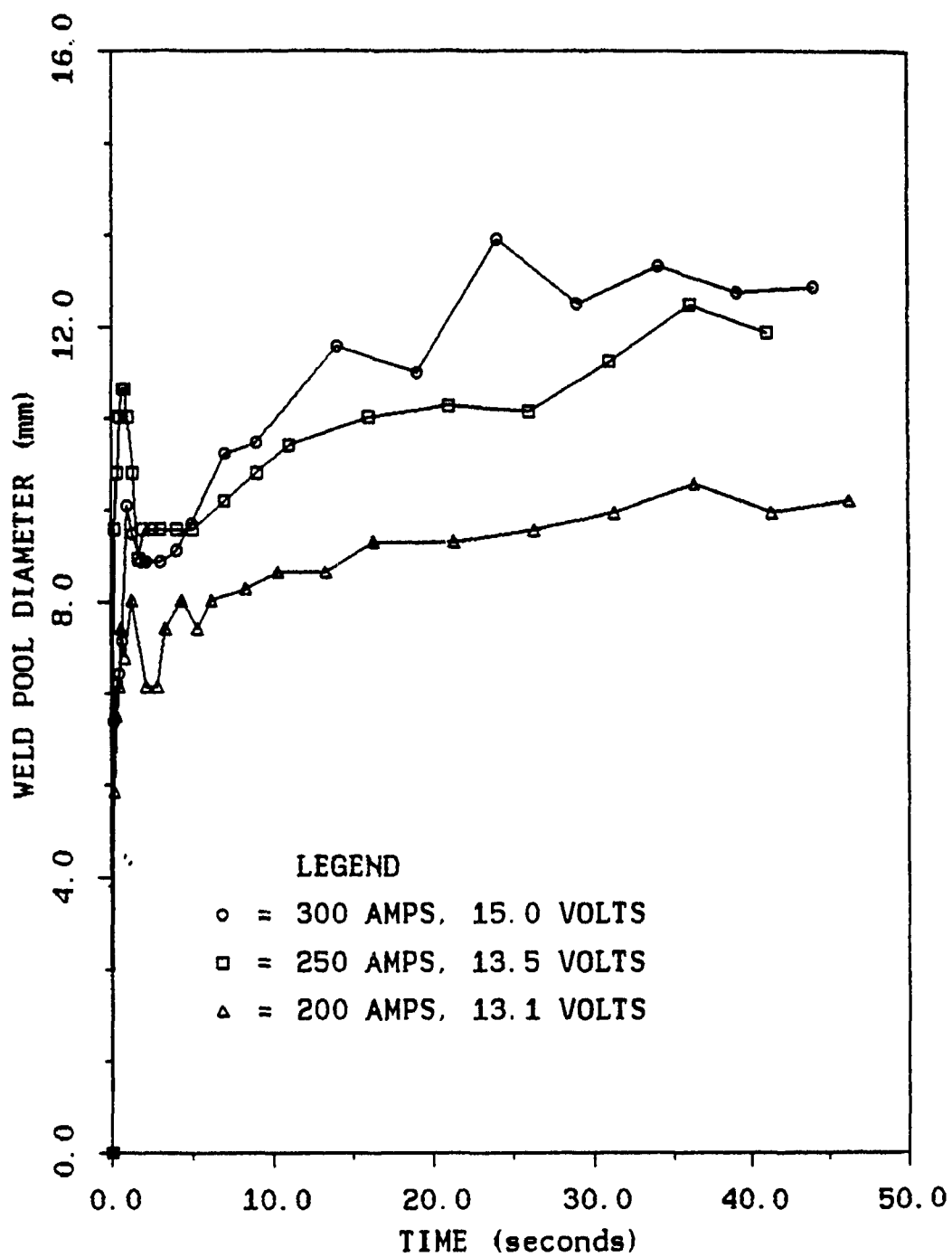


Figure 10. Weld Pool Growth With Time. 90° Electrode Tip Angle. 5 mm Arc Length.

20] three-dimensional heat flow solution supports larger weld pools with increasing power. Solving for radius of weld pool while setting velocity equal to zero gives

$$r = \frac{q}{2\pi K(T_m - T_o)}$$

Assuming constant properties, input power is linearly related to weld pool size.

2. Effect of Arc Length Changes

Three arc lengths (3 mm, 4 mm, and 5 mm) were studied using different input power and electrode tip angles. The effect of arc length is not clearly discernable as seen in Figure 11. Scattered data was obtained due to voltage fluctuations. Instrumentation only allowed for constant current settings, not constant power. As arc length increased, voltage increased to maintain current levels. This always increased power input to the weld resulting in scattered data. Figure 11 does show 4 mm arc lengths do produce slightly larger weld pools.

3. Effects of Electrode Tip Angle

Three electrode tip angles as shown in Figure 12 were studied. Tip angles 20°, 45°, and 90° were used as input power and arc length were varied. Unlike the effect of arc length, the effect of differing electrode tip angles can clearly be seen in Figure 13. 20° electrode tip angles produce the

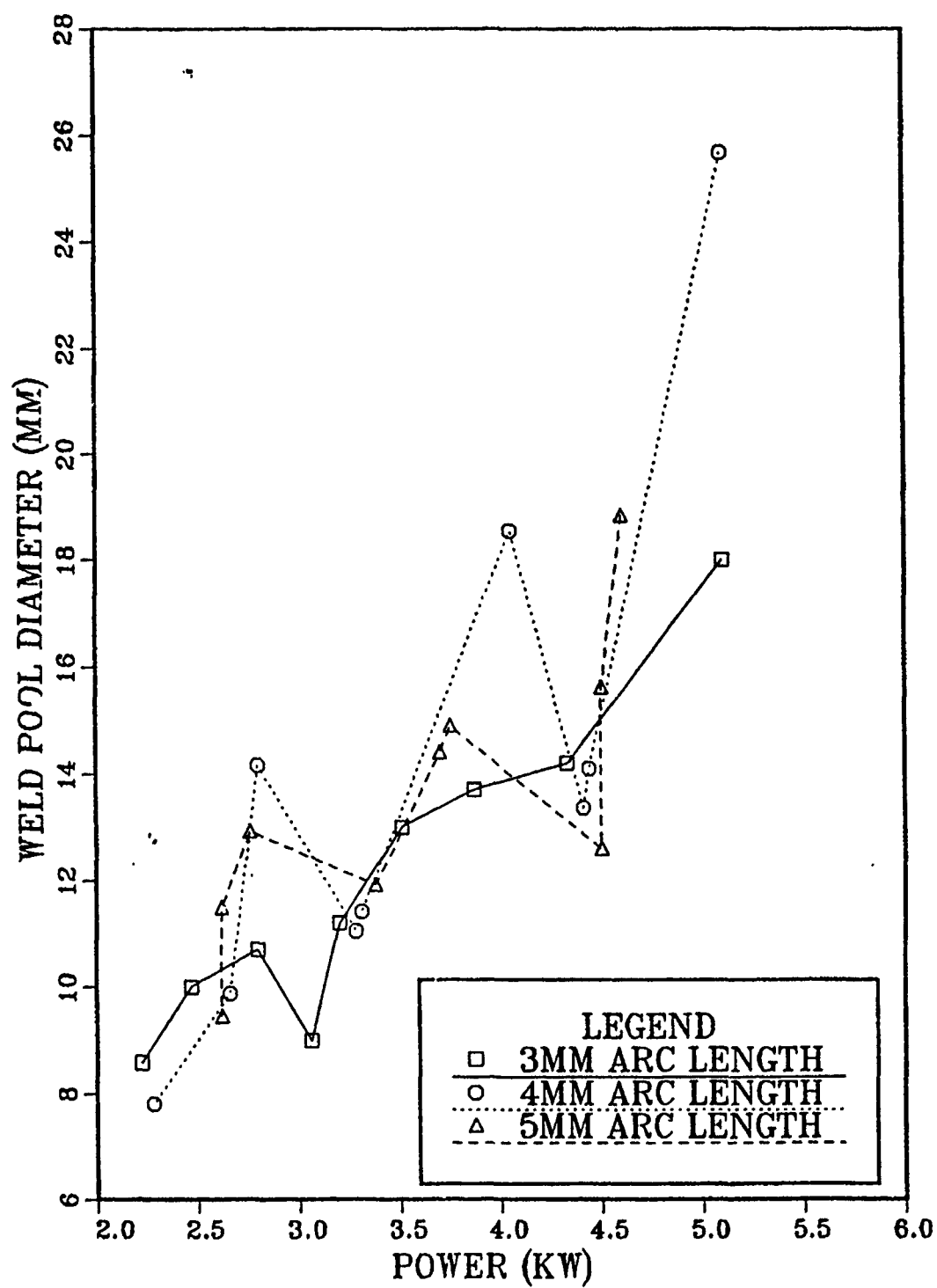


Figure 11. Effect of Changes in Arc Length.

largest pool, followed by 45°, and the smallest weld pools were produced by 90° electrode tip angles.

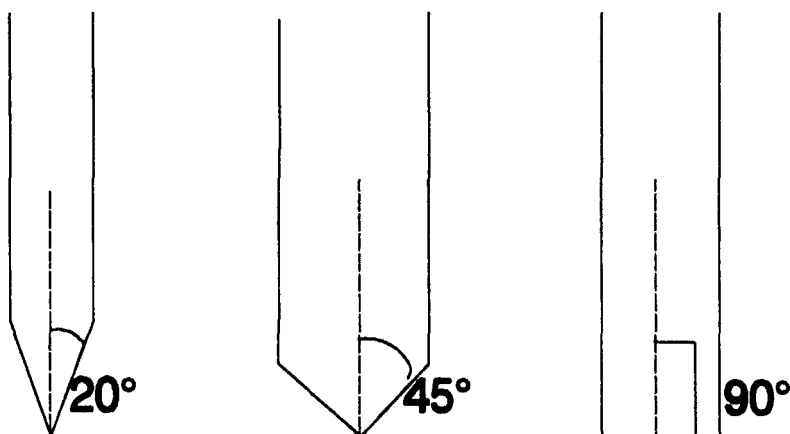


Figure 12. Electrode Tip Angles.

D. WELD POOL OBSERVATIONS

It is essential that correct mathematical models describing convection and heat flow in weld pools are utilized prior to full automation of the welding process. In Chapter I, Table I reviews selected numerical models and Table II reviews selected experimental studies. This section will compare current weld pool observations with those listed in Tables I and II. A number of discrepancies between the models and computational predictions were found as described below.

1. Weld Pool Rise

One of the most clear and distinct observations that the vision system used has made possible to measure is weld pool rise during GTA welding of steels. A weld pool rise at

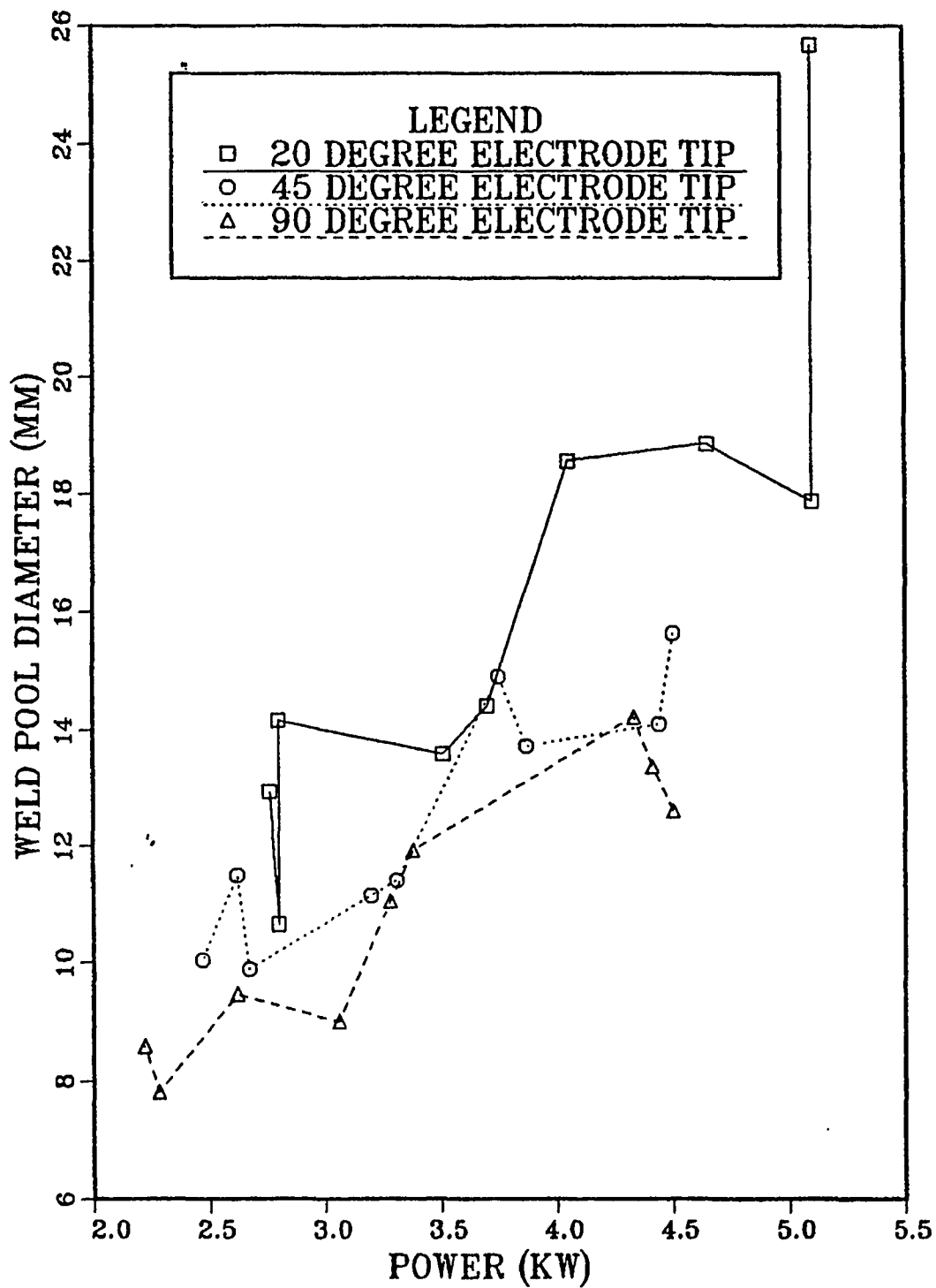
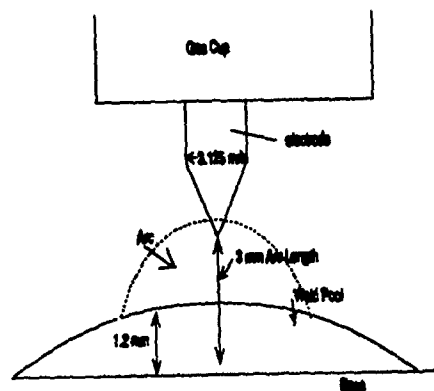


Figure 13. Effect of Changes in Electrode Tip Angle.

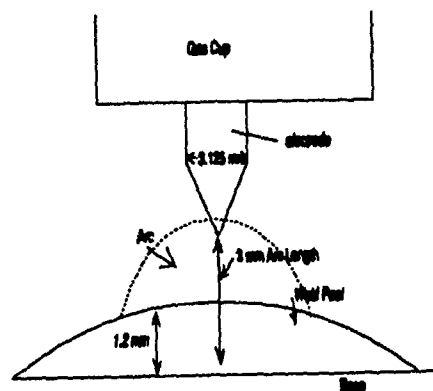
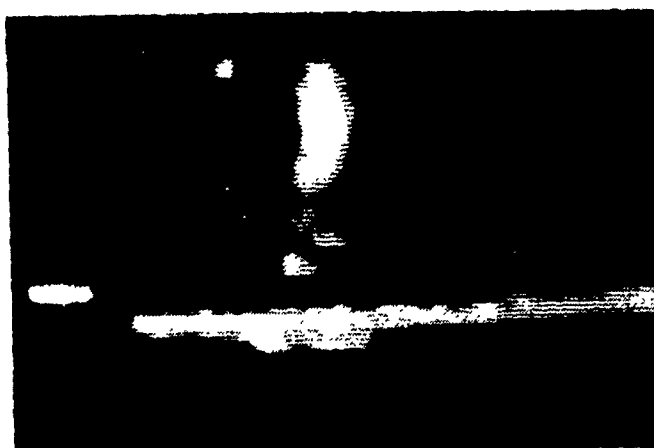
the center of up to 1 3/4 mm was observed. All of the selected studies [Refs. 1, 2, 4, 6, 7] except Zacharia et al. [Ref. 5] in Table I either neglect this rise or assume a flat surface. Zacharia et al.'s model does treat the surface as truly deformable; however his model predicts a crown like surface. The present experiments show a clear rise of the entire weld pool including the center as shown in Figure 14. An experimental study by Kraus [Ref. 12] does confirm the weld pool profile shown by the vision system. However, Kraus' measurements were only made after the arc had been extinguished. He also attributes this rise in part to the removal of arc impingement associated with the cessation of the arc. Other experimental studies as listed in Table II [Ref. 9, 10, 13] were not using visualization techniques capable of observing weld pool rise. Weld pool rise observed increased with power and does not appear to be related to electrode tip angle or arc length as seen in Figures 15 and 16.

2. Flow Observations

All computational models listed in Table I predict an inward or outward flow on the weld pool surface. Most of the studies listed attribute the flow to the three driving forces: electromagnetic, buoyancy, and surface tension. The vision system shows a distinct circumferential flow. Welding surfaces were seeded with alumina particles and these particles were



a. Time + 0 Seconds



b. Time + 2 Seconds

Figure 14. Weld Pool Rise, 1.2 mm, 300A, 14.8v, Arc Length 3mm, 45° Electrode Tip Angle. Weld Pool Diameter 14.1 mm. Enlargement x5.0.

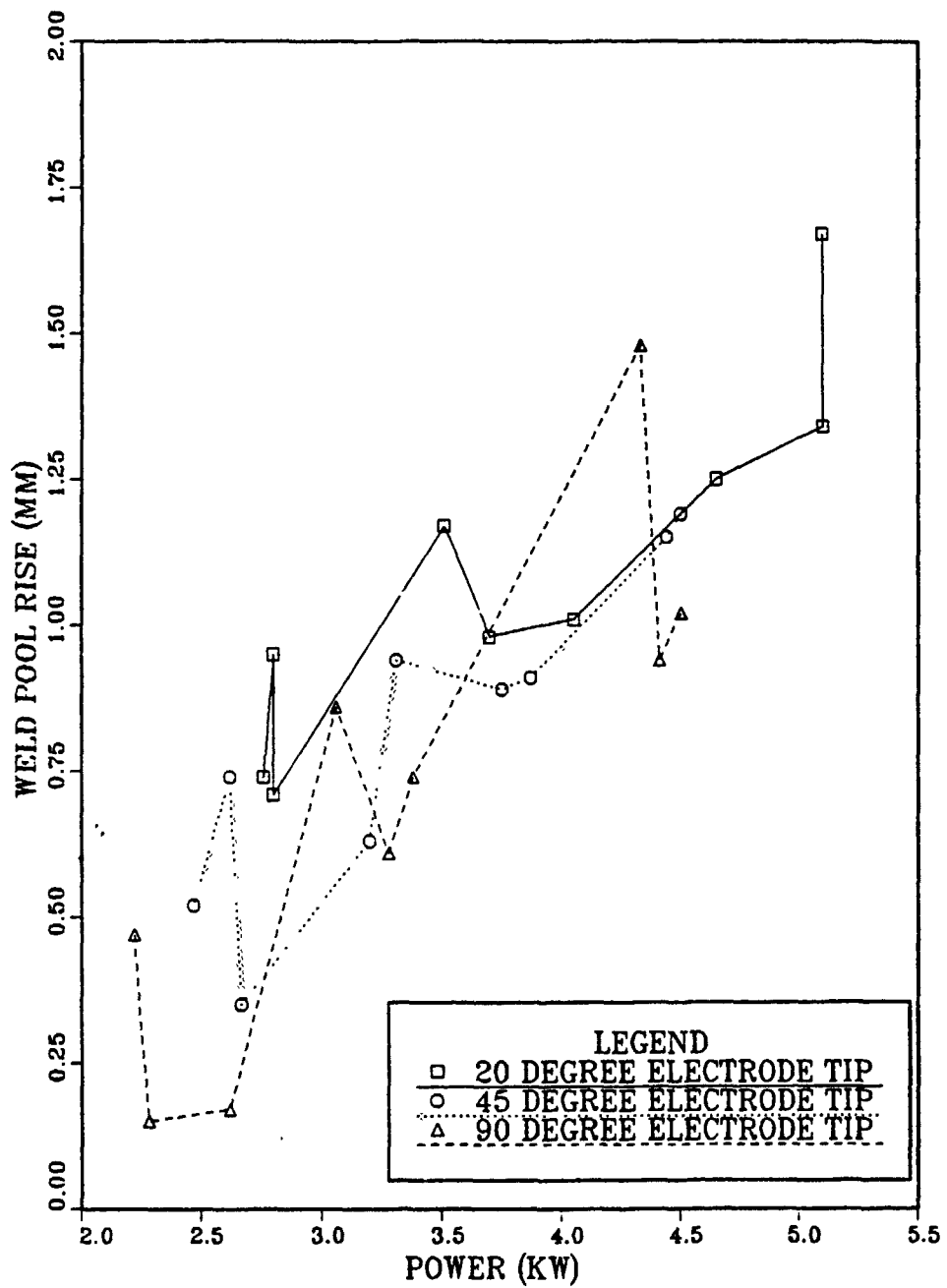


Figure 15. Weld Pool Rise for Various Power Levels and Electrode Tip Angle.

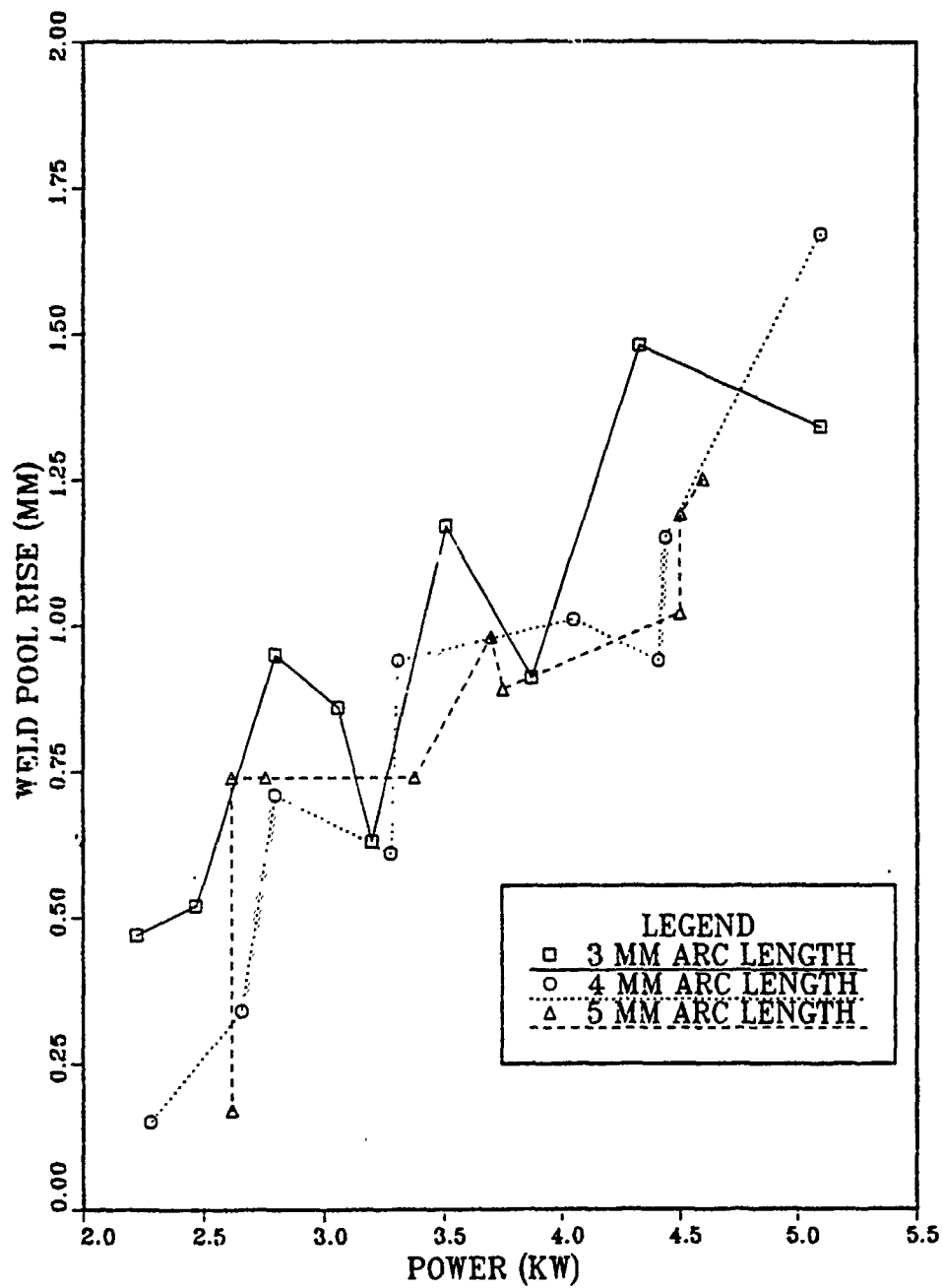


Figure 16. Weld Pool Rise for Various Power Levels and Arc Lengths.

videotaped floating on the surface of weld pools in a mainly clockwise direction. Figure 4 shows a distinct clockwise flow. These circular flows occasionally reversed directions completely and were often irregular in nature. In the experimental studies review listed in Table II, only Woods and Milner [Ref. 9] report swirling flow in what appeared to be the clockwise direction. Metcalfe and Quigley [Ref. 10] using cine photography report seeing floating material on the weld pool but do not report the flow direction. The present weld pool visualization technique did not allow flow patterns to be categorized according to input power, arc length or electrode tip angle since rotation was observable in most experiments. When rotation was not observed, it was always due to the absence of floating impurities. Counter-clockwise rotation was often viewed when welding within two inches from the edge of the plate as noted in Section B of this chapter.

3. Weld Pool Oscillations

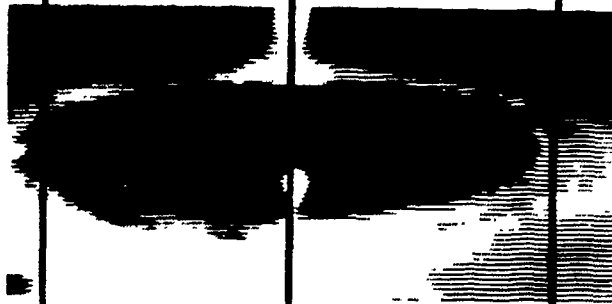
Oscillations were observed for all welding conditions. Oscillations in shape, size, and centering of the weld pool were clearly observable. These are also contrary to the predicted steady weld pools of the selected computational studies [Refs. 1 through 7]. Current models do not account for this phenomena nor have experimental studies [Refs. 9, 10, 12] brought this out. Selected video frames displaying weld pool oscillations are presented in Figures 17a through 17c.

Lines are for reference only

a. Time
+ 0 Seconds



b. Time
+ 1 Second



c. Time
+ 3 Seconds

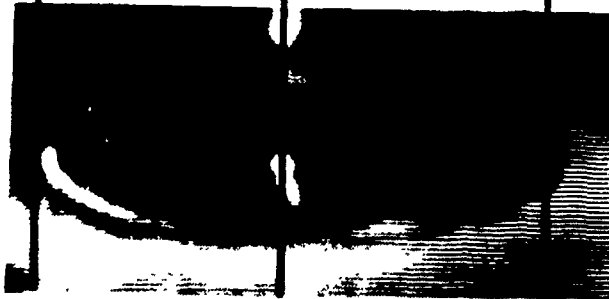


Figure 17. Weld Pool Oscillations, 200A, 14.0v, 4mm Arc Length, 20° Electrode Tip Angle. Weld Pool Oscillates From Right (a) to Left (b) Back to Right (c). Enlargement x5.0.

**TABLE VI. COMPREHENSIVE LISTING OF
STATIONARY ARC EXPERIMENTS**

Tip (degree)	V (Volts)	I (Amps)	Power (Kwatts)	Arc Length (mm)	Weld Pool Diameter (mm)	Weld Pool Rise (mm)	Weld Pool Depth (mm)
20	14.0	200	2.80	3	10.7	1.0	
20	14.0	251	3.51	3	13.6	1.2	
20	17.0	300	5.10	3	17.9	1.3	
20	14.0	200	2.80	4	14.2	0.7	
20	16.2	250	4.05	4	18.5	1.0	
20	17.2	300	5.16	4	25.7	1.7	
20	13.8	200	2.76	5	12.9	1.7	
20	14.7	252	3.70	5	14.4	1.0	
20	15.5	300	4.65	5	18.8	1.3	
45	12.3	201	2.47	3	10.0	.5	
45	12.9	248	3.20	3	11.2	.6	
45	12.9	300	3.87	3	13.7	.9	8.3
45	13.2	202	2.07	4	9.9	.3	7.0
45	13.2	251	3.31	4	11.4	.9	6.7
45	14.8	300	4.44	4	14.1	1.2	8.5
45	13.1	200	2.62	5	11.5	.7	
45	15.0	250	3.75	5	14.9	.9	
45	15.0	300	4.50	5	15.6	1.2	1.1
90	11.1	200	2.22	3	8.6	.5	5.0
90	12.2	251	3.06	3	9.0	.9	6.5
90	14.3	303	4.33	3	14.2	1.5	8.0
90	11.4	200	2.28	4	7.8	.2	
90	13.1	250	3.28	4	11.1	.6	
90	14.7	300	4.41	4	13.4	.9	
90	13.1	200	2.62	5	9.5	.2	
90	13.5	250	3.38	5	11.9	.7	
90	15.0	300	4.50	5	12.6	1.0	

IV. MOVING ARC EXPERIMENTS

Bead on plate welds ten inches long were studied for the effect of welding speed and input power variations on weld pool flow patterns. Two general power settings and four welding speeds were studied. Arc length and electrode tip angle were held constant at 4mm and 45° respectively. After the selection of a power level, the video recorder was started, the arc struck and the plate set in motion. Measurements of the weld pool dimensions were taken from both a cross-section of the solidified weld bead and video of the weld pool. Welding parameters and weld pool dimension were utilized to calculate welding efficiencies for moving arc GTA process. The video recordings were also utilized to study weld pool surface flows. A summary of welding parameters and weld pool measurements for the various experimental runs can be found in Table VIIA and B.

A. WELDING EFFICIENCY

Using Rosenthal's [Ref. 20] point source heat flow solution the welding efficiency (η) is obtained as:

$$\eta = \frac{2\pi (T_m - T_o) K r_o}{IE} \exp \frac{v (r_o + x)}{2\alpha} \quad (5)$$

**TABLE VIIA. SUMMARY OF WELDING PARAMETERS
AND WELD POOL MEASUREMENTS**

I Amps	V Volts	P Watts	Speed mm/s	Weld Pool Width mm	Weld Pool Length mm	% Ahead Arc	% Behind Arc	Weld Pool Depth mm
200	14.4	2880	.85	10.5	16.3	40.0	60.0	
				10.0	16.5	38.2	61.8	
				9.9	16.0	39.1	60.9	
				10.3	16.2	38.9	61.1	
				10.2	16.1	39.5	60.5	
200	14.8	2960	2.27	9.1	13.5	36.1	64.9	
				8.9	13.6	34.9	65.1	
				9.3	13.0	34.9	65.1	
				9.0	13.4	35.0	65.0	
				9.2	13.2	35.2	64.8	
				9.3	13.1	35.3	64.7	
200	13.9	2780	3.22	8.0	9.4	33.3	66.7	2.8
				8.1	9.3	34.0	66.0	
				7.8	9.0	34.2	65.8	
				7.9	9.1	32.9	67.1	
				8.1	9.7	34.1	65.9	
				8.2	9.6	32.5	67.5	
200	13.7	2740	4.17	7.4	8.3	30.1	69.9	
				7.3	8.0	29.4	70.6	
				7.2	8.4	29.8	70.2	
				7.3	7.9	29.5	70.5	
				7.6	8.1	29.6	70.4	
				7.3	8.2	29.4	70.6	
				7.5	8.1	29.7	70.3	

**TABLE 11B. SUMMARY OF WELDING PARAMETERS
AND WELD POOL MEASUREMENTS**

I Amps	V Volts	P Watts	Speed mm/s	Weld Pool Width mm	Weld Pool Length mm	+ Ahead Arc	+ Behind Arc	Weld Pool Depth mm
250	14.3	3580	.85	11.00	19.2	43.8	56.2	5.5
				11.2	18.9	42.1	57.9	
				11.1	19.1	43.9	56.1	
				10.9	19.1	44.1	59.9	
250	14.2	3550	2.27	9.7	16.4	35.5	64.5	3.6
				9.4	15.9	36.1	63.9	
				9.9	16.1	36.0	64.0	
				10.0	16.3	35.0	65.0	
				9.6	16.2	35.9	64.1	
250	14.4	3600	3.22	8.5	12.5	26.9	73.1	3.0
				8.3	12.1	25.8	74.2	
				8.2	13.0	26.0	74.0	
				8.6	12.4	26.3	73.7	
				8.5	12.4	27.4	72.6	
				8.4	12.6	28.0	72.0	
250	14.0	3500	4.17	8.0	11.5	23.1	76.9	2.1
				8.1	11.3	23.9	76.1	
				8.2	11.8	22.5	77.5	
				7.9	11.9	22.1	77.9	
				7.8	11.0	22.6	77.4	
				8.1	11.4	23.5	76.5	

where K , T_m , T_o , r_o , I , E are listed in Chapter III
 and v = welding speed
 α = thermal diffusivity

v and x are in the coordinate system shown in Figure 18.

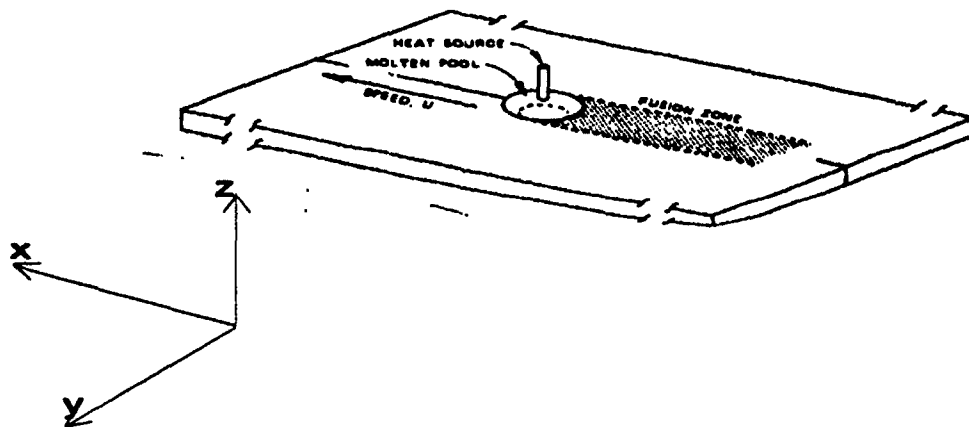


Figure 18. Coordinate System.

Using Equation (5) and measurements of actual weld pool dimensions from both video and solidified weld pool, efficiency can be calculated. Weld pool cross-section samples were prepared as noted in Chapter III (seen in Figure 3) and provided weld pool depth and width measurements with an uncertainty of 0.2mm. Measurement of weld pool length dimension were taken directly from video screen while reviewing each frame. The electrode tip or gas cap was utilized as a basis for comparison measurements and also resulted in an uncertainty of 0.2mm. Table VIII lists the efficiencies as calculated from Equation (5), using measurements taken from the front, side, rear, and bottom of the weld pool. Efficiencies calculated with dimensions from

the front of the weld pool provided the poorest results. Some values above 100% were obtained indicating that Rosenthal's point source solution may be a poor representation of the fusion zone size. Efficiencies calculated from dimensions of the front, rear, and bottom decreased with increasing speed while efficiencies calculated from dimensions of the side increased with increasing velocity.

Using calorimetric type measurements, Giedt et al. [Ref. 22] measured an efficiency of 80% for welding 304L stainless steel with parameters listed in the first line of Table VIII. His measurements show a decreasing efficiency above 200 Amp (2.0 KW). Comparison with the calculated efficiency from weld pool depth measurements in Table VIII shows a similar decreasing efficiency trend with increasing power.

TABLE VIII. CALCULATED EFFICIENCIES.

Power Kwatts	Speed mm/sec	% Front	% Rear	Efficiency		Giedt et al.** % Cal
				% Side	% Bottom	
2.05	.85	***				80
2.88	.85	***	100	66.3		
2.96	2.27		86.4	80.22		
2.78	3.22	85	75	88.2	77.7	
2.74	4.17	77	62.1	93.4		
3.58	.85	***	88.8	59.8	76.0	
3.55	2.27	***	86.4	74.6	73.8	
3.60	3.22	77.7	75.0	75.4	71.5	
3.50	4.17	75.4	74.5	86.8	69.6	

* Based on Equation (5) using measurements from Table VII.

** Based on Giedt et al.'s [Ref. 23] measurements using calorimetric type experiments. Giedt et al.'s data indicate an efficiency drop beyond 200 Amp (2.0 Kw).

*** Values above 100% indicating Rosenthal's point source solution is poor representation of the fusion zone size.

B. EFFECT OF WELDING POWER

Two different power settings were utilized for moving arc experiments. 200 and 250 amps along with 13.7 to 14.7 volts were used to provide the two general power ranges. The higher power range 3590 ± 100 W and the lower power range 2840 ± 120 W were both generated while the arc length of 4mm and electrode tip angle of 45° remained constant throughout the experiments. Weld pool dimensions were tabulated as noted in section A of this chapter and graphed against input welding power. Each experiment was grouped according to welding speed.

Figures 19-21 show one clear effect of input power. The higher the input power, the larger the weld pool as noted by a wider and longer weld pool. As for stationary welds, Rosenthal's [Ref. 20] three-dimensional heat flow solution also supports larger weld pools with increasing power. Each jump in power shown in Figures 19-21, shows an increase in weld pool length, width, and depth.

C. EFFECT OF WELDING SPEED

Four different welding speeds (0.85, 2.27, 3.22 and 4.17 mm/s) were utilized to study moving arc welding. In both high and low power welds measurements of weld pool dimensions were taken from video or solidified weld bead, as stated earlier. Rosenthal's moving point source solution may be rearranged to show how welding velocity effects weld pool dimensions. Equation (6) shows that at the rear of the weld pool where

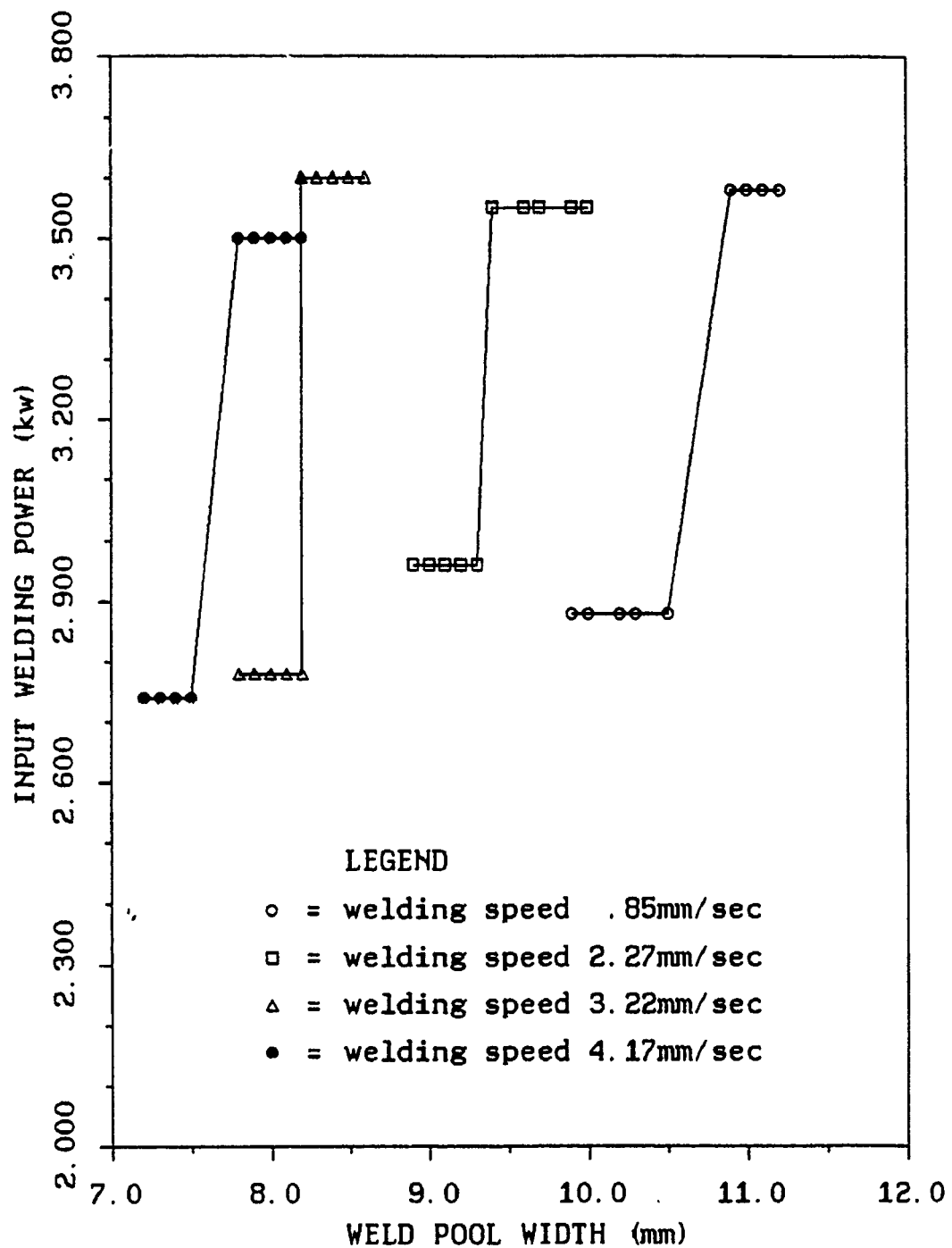


Figure 19. Effect of Input Power. Larger Input Powers Produce Larger Welds.

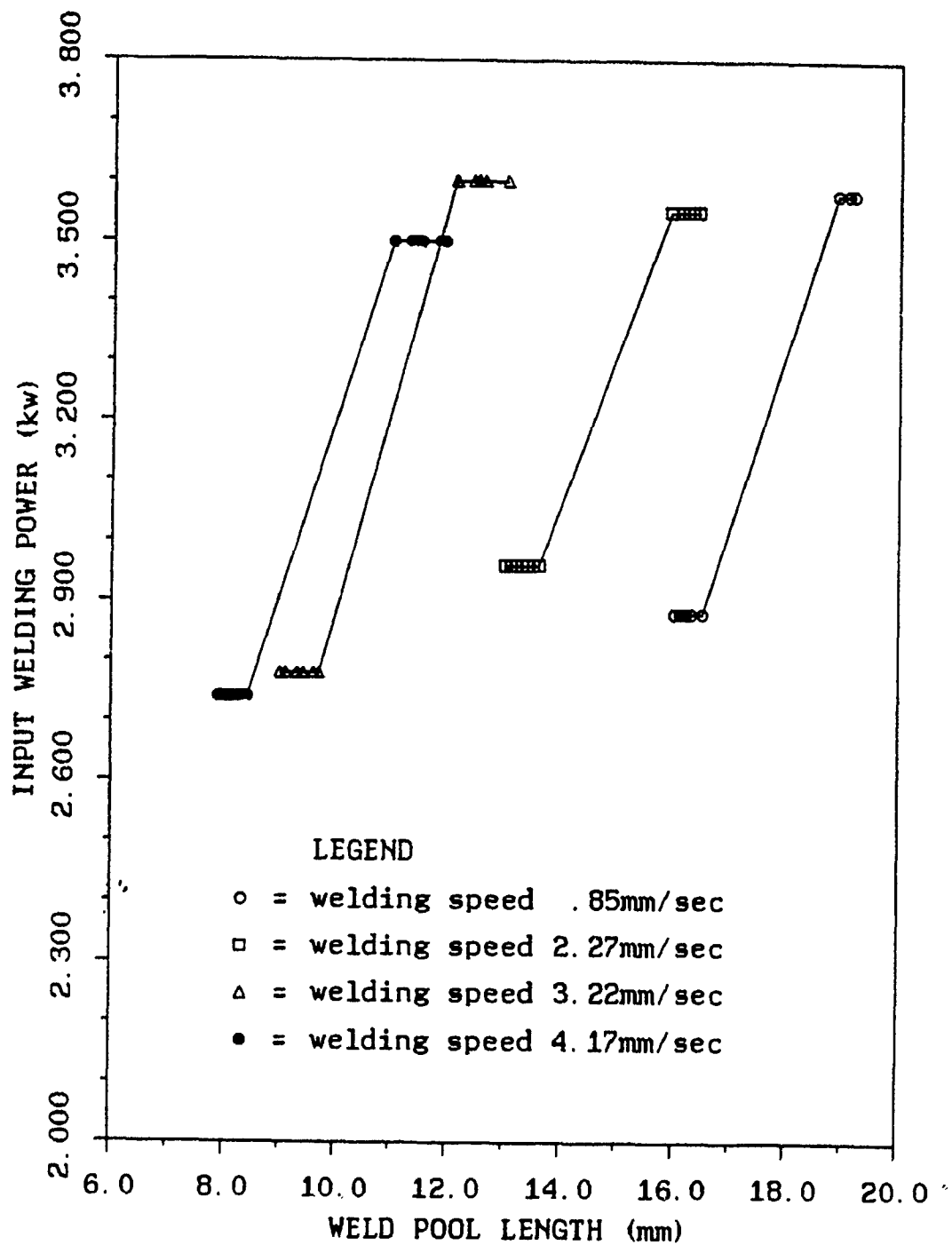


Figure 20. Effect of Input Power. Larger Input Powers Produce Larger Welds.

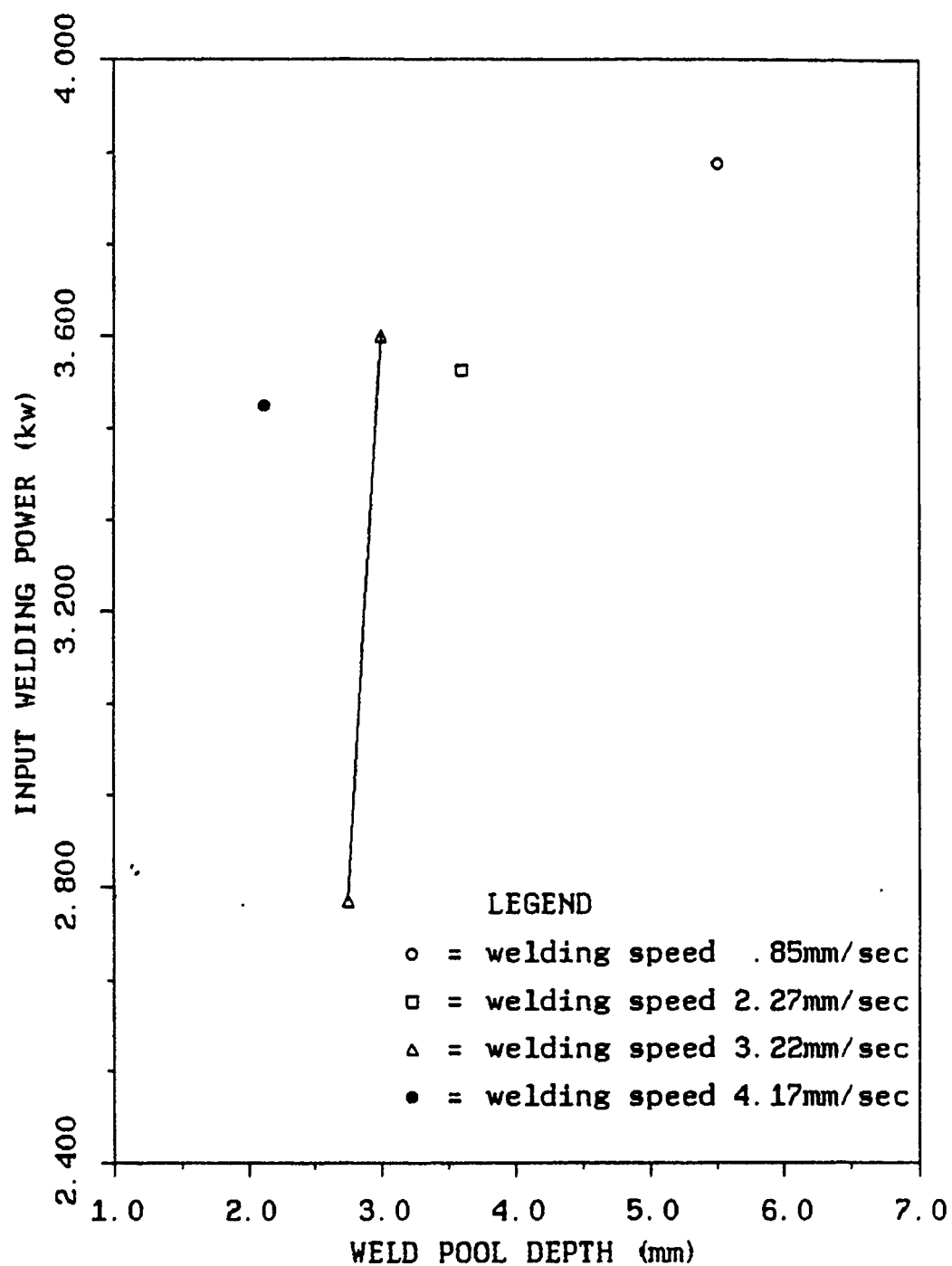


Figure 21. Effect of Input Power. Larger Input Powers Produce Larger Welds.

$y=0$, $z=0$, and $r_0=|x|$

$$q = 2\pi (T_m - T_o) |x| \exp \frac{v (|x| + x)}{2\alpha_s} \quad (6)$$

Also, the rear of the weld pool $|x| + x = 0$, showing that the dimension of the moving arc weld pool is a linear function of power. Table IX shows calculated weld pool dimensions using Rosenthal's moving point source solution. The values incorporate a welding efficiency of 80% for the listed welding parameters. Weld pool dimensions decrease as welding speed increases given by weld pool width and length decreases. Since the distance between the center and rear of the weld pool is determined by the input power, a decrease in weld pool length can be attributed to a decrease in the weld pool in front of the arc. This causes the percent of total weld pool area in front of the arc to decrease with increasing speed, as shown in Figures 22 through 27.

Using a numerical model Ule et al. [Ref. 8] predict weld pool measurements for an actual input power of 2.54 Kw and welding speed of 4mm/sec. His values are listed at the bottom of Table IX and are somewhat larger than the corresponding measurements for a slightly higher power of 2.74 Kw.

D. WELD POOL SURFACE FLOWS AND FEATURES

Several new features of the weld pool have been made observable with the laser vision system. Surface flow patterns were not as clearly observable as for stationary arc

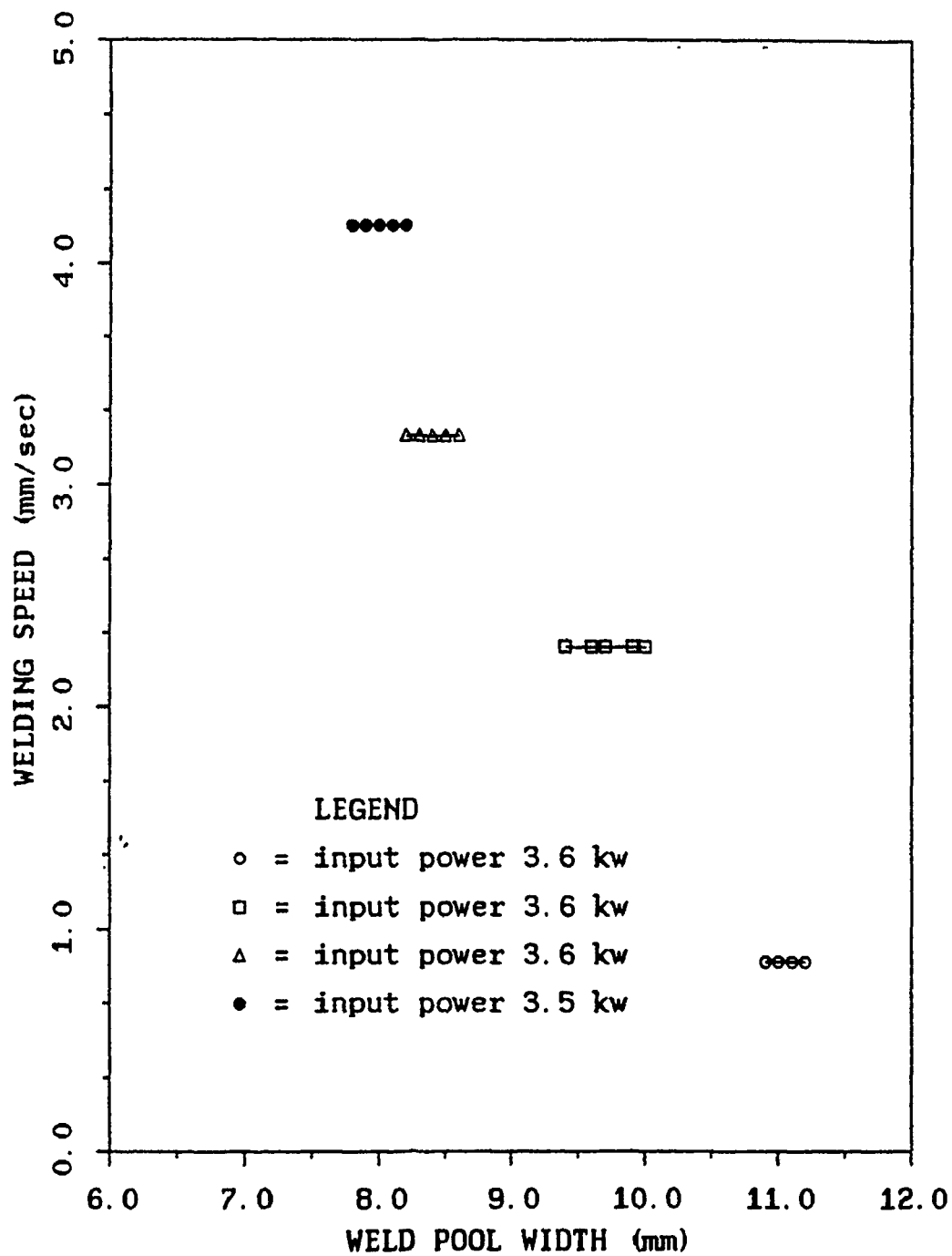


Figure 22. Effect of Welding Speed. Faster Moving Arc Welds Produce Smaller Weld Pools.

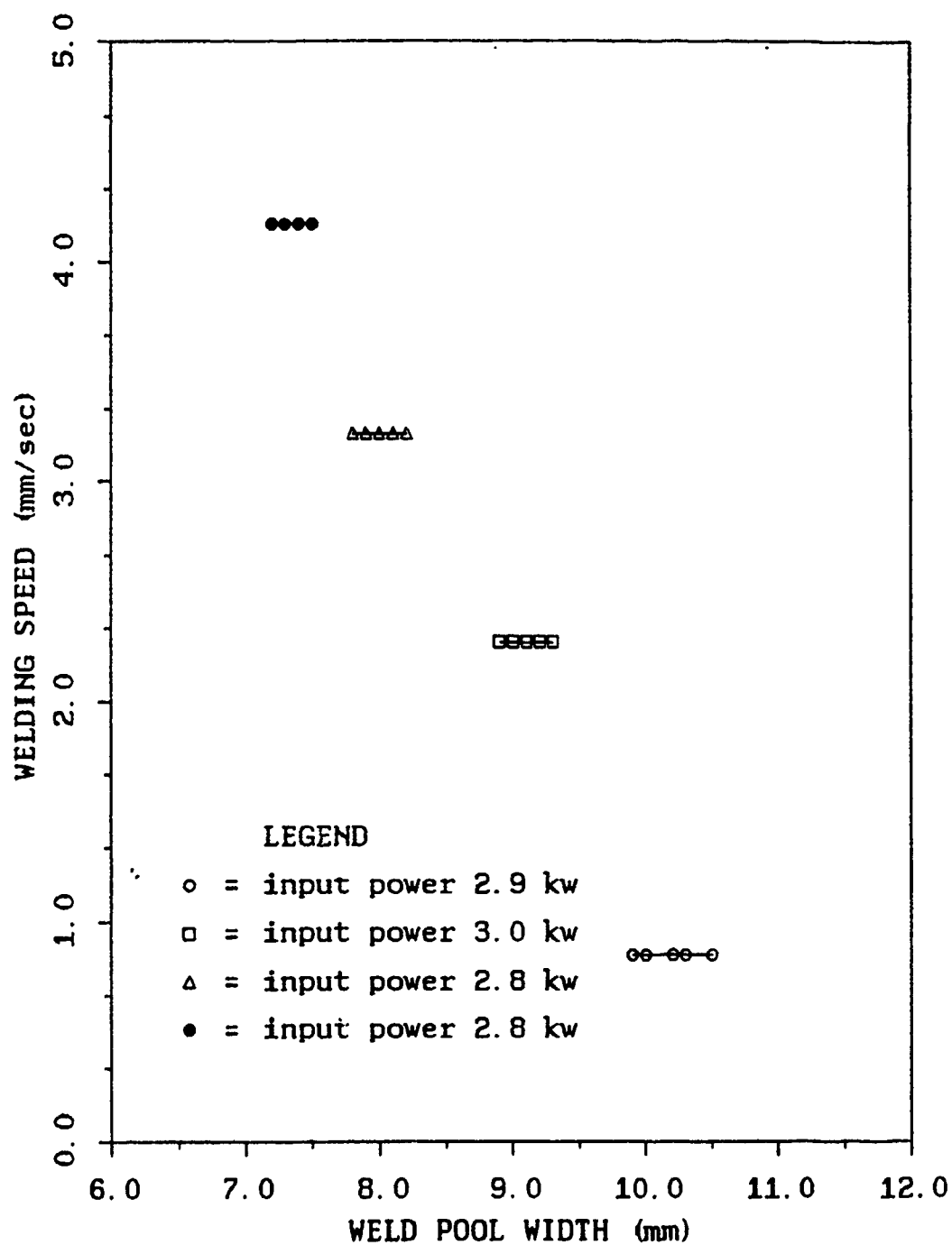


Figure 23. Effect of Welding Speed. Faster Moving Arc Welds Produce Smaller Weld Pools.

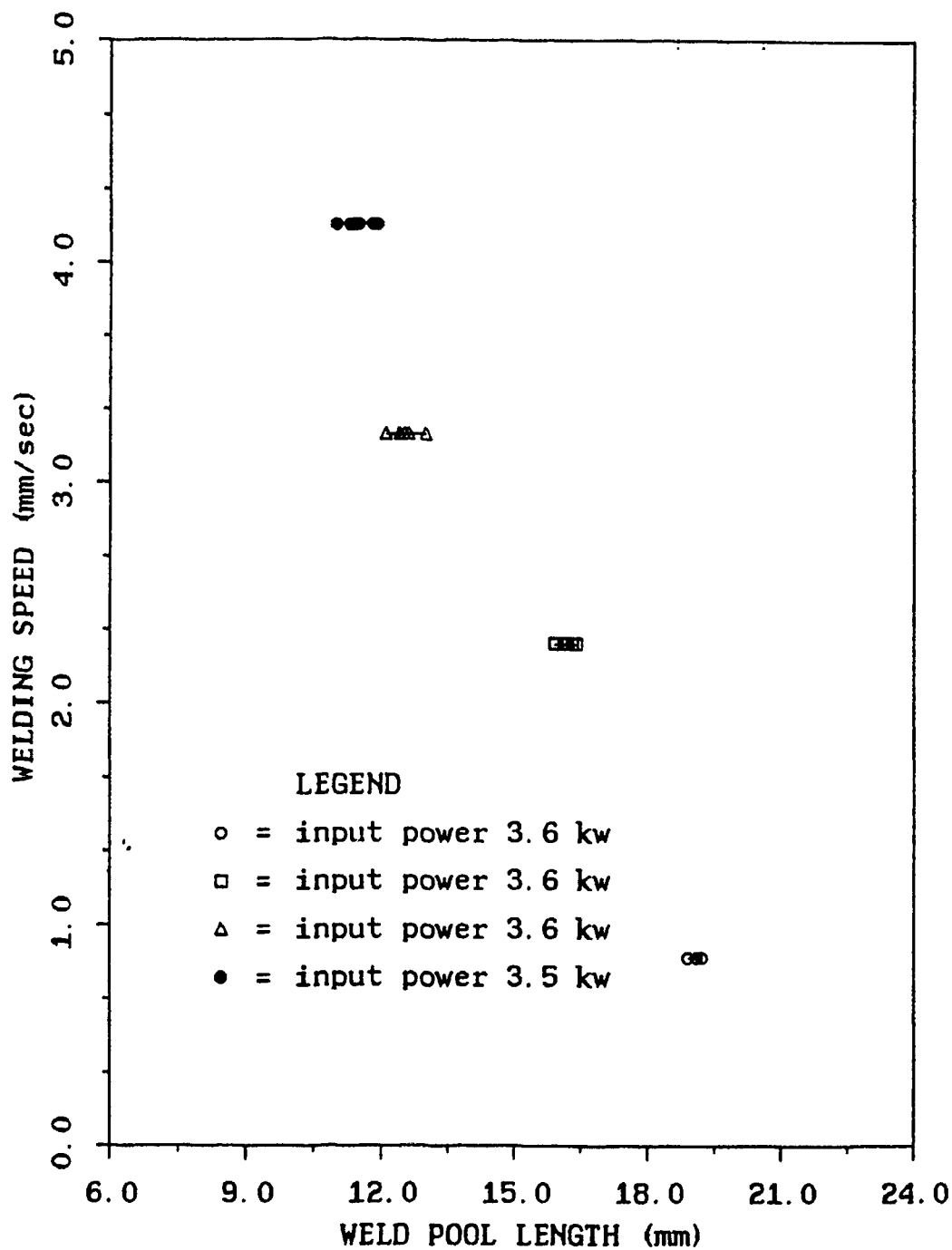


Figure 24. Effect of Welding Speed. Faster Moving Arc Welds Produce Smaller Weld Pools.

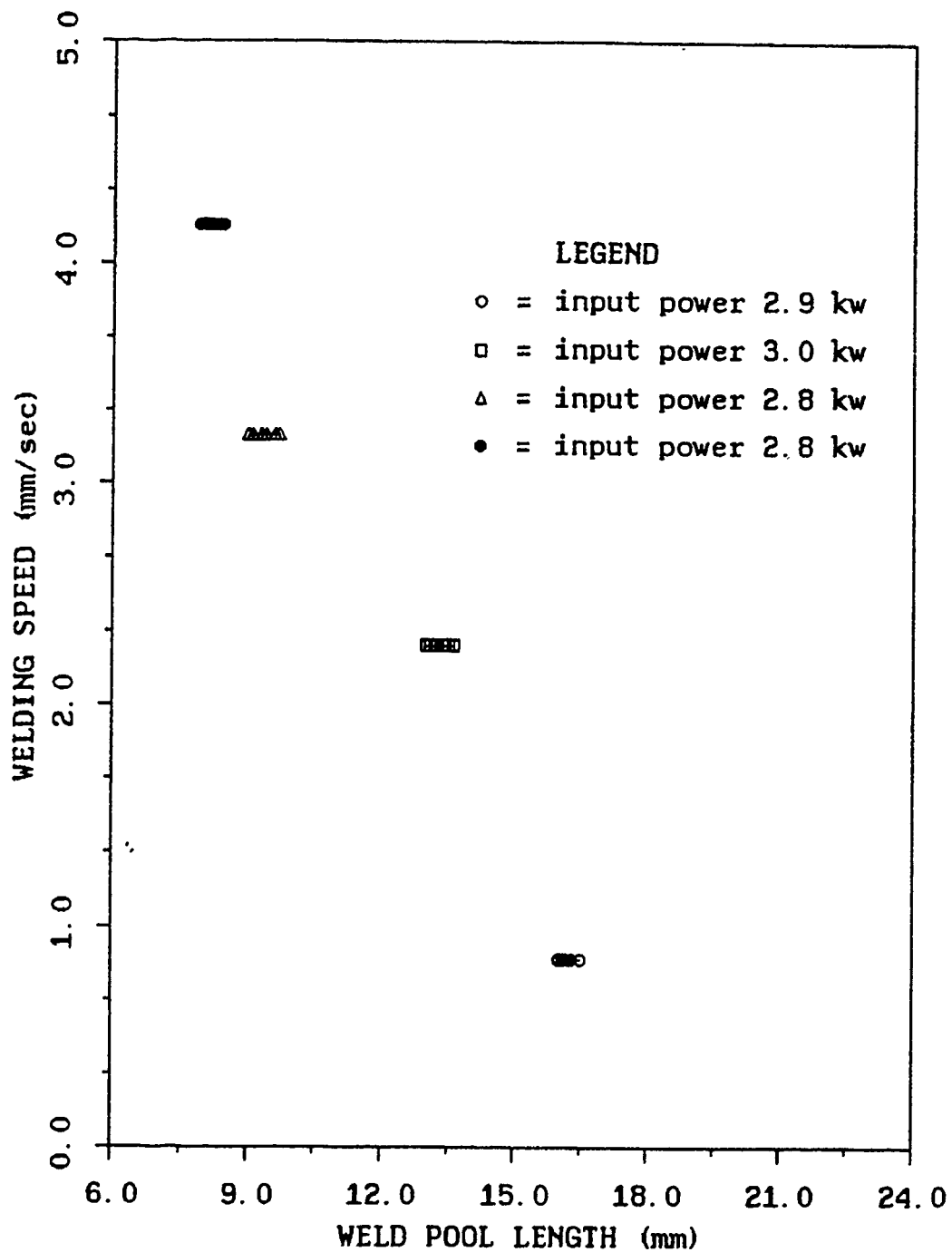


Figure 25. Effect of Welding Speed. Faster Moving Arc Welds Produce Smaller Weld Pools.

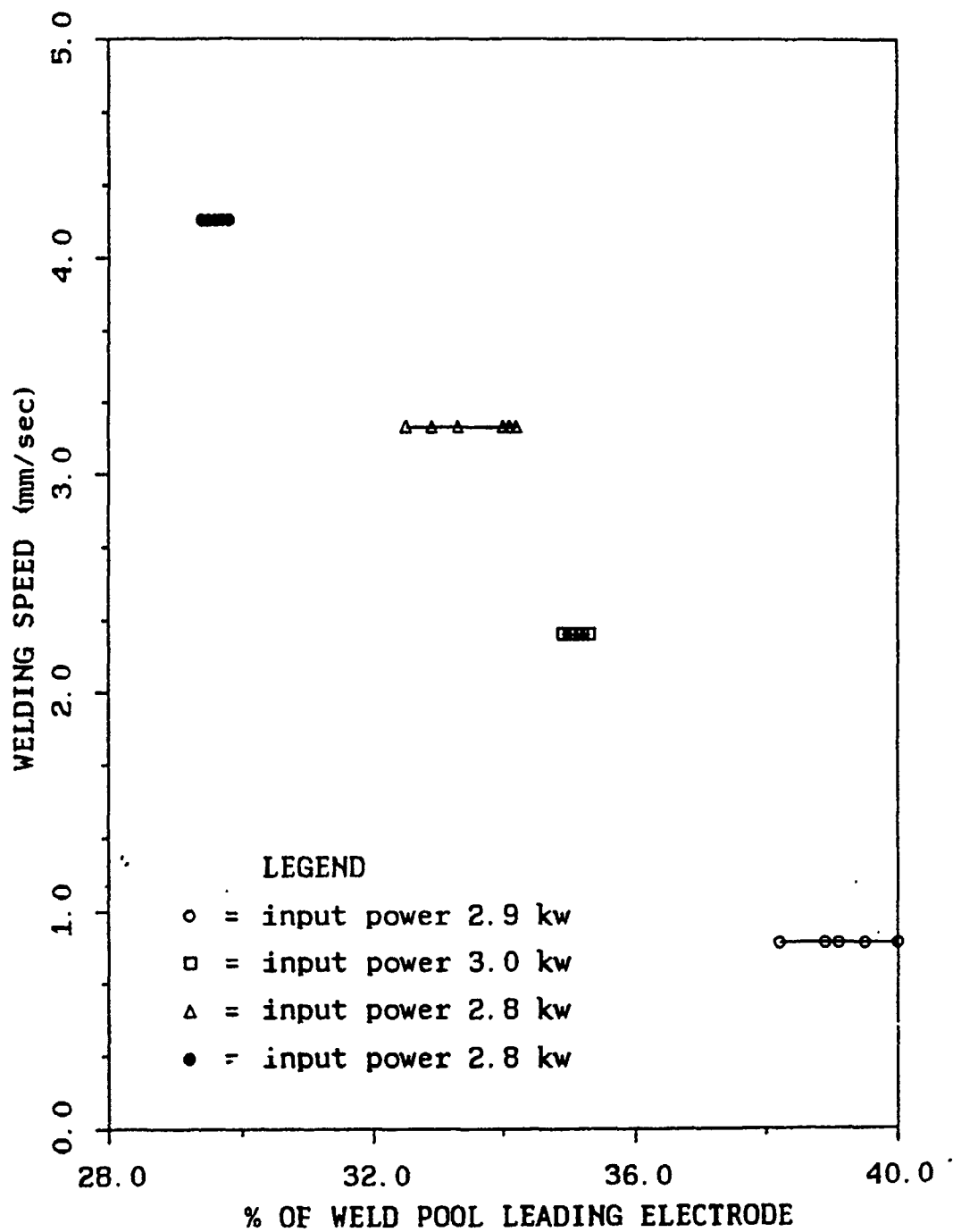


Figure 26. Effect of Speed on % of Weld Pool Leading Arc. Faster Moving Arc Welds Have Small % of Weld Pool Leading Arc.

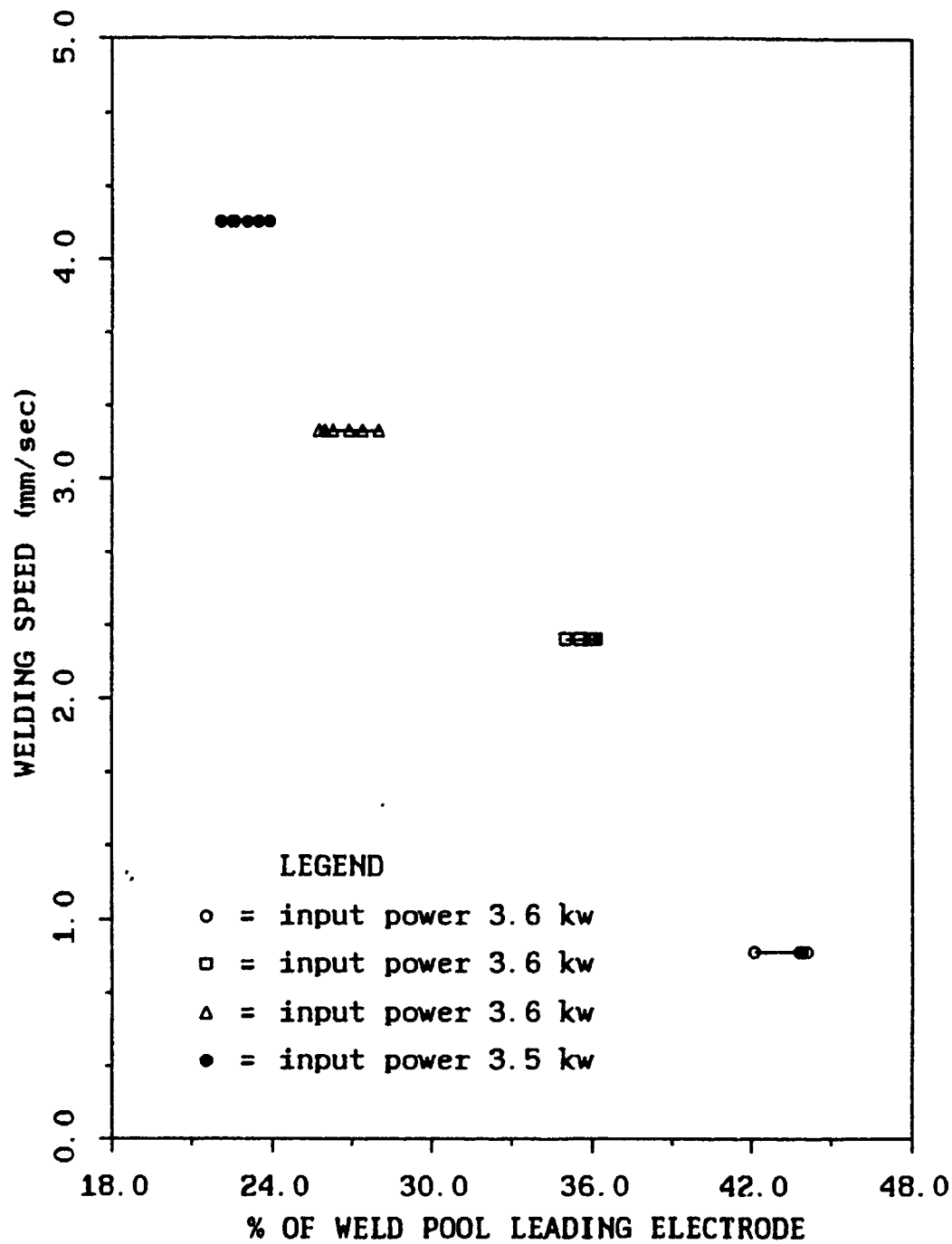


Figure 27. Effect of Speed on % of Weld Pool Leading Arc. Faster Moving Arc Welds have Small % of Weld Pool Leading Arc.

TABLE IX. CALCULATED WELD POOL DIMENSIONS.

Calculated from Rosenthal for 80% efficiency (Actual measured value).

Power KWatts	Speed mm/sec	Weld Pool Width mm	Weld Pool Length mm	Weld Pool in Front of Elec mm
2.88	.85	10.6 (10.1)	12.7 (16.2)	38.6 (39.1)
2.96	2.27	9.1 (9.1)	11.4 (13.3)	29.8 (35.2)
2.78	3.22	7.6 (8.1)	10.3 (9.4)	23.0 (33.6)
2.74	4.17	6.3 (7.4)	9.9 (8.1)	24.6 (29.8)
3.58	.85	14.0 (11.1)	15.4 (19.1)	36.9 (43.8)
3.55	2.27	10.2 (9.8)	13.4 (16.2)	28.0 (35.5)
3.60	3.22	8.9 (8.4)	13.0 (12.4)	24.6 (26.9)
3.50	4.17	7.8 (8.1)	11.2 (11.7)	22.3 (23.1)
2.54*	4.0	8.9	12.3	24.2

* Based on Uie's [Ref. 8] computer model.

experiments due to the relatively slow recording speed of 60 frames per second. Some of the clearly observed features are next presented.

1. Weld Pool Depression and Rise

A weld pool depression near the electrode estimated to be about 1-2mm was present in all moving arc welds. This depression is centered under the electrode and causes a rise near the tail end of the weld pool. Figure 28 shows this depression and rise. Most solidified weld beads exhibited this rise shown in Figure 29. During production welding, tabbing is commonly used on either end of butt weld to start and finish the weld. This prevents loss of material strength due to formation of depression when abruptly extinguishing the arc.

The sequence of Figures 28a-d shows this depression when the arc is extinguished abruptly.

2. Weld Pool Surface Flows

As stated earlier, photography of weld pools from a TV monitor, replayed on a time lapse recorder allowed frames to be taken at representative speed of $1/60$ of a second. This speed provides excellent video of the weld pool in motion making still photographs a poor substitute for viewing the welding process at its actual speed. Indeed the best video and consequently the best still photographs were produced using low welding power at low welding speeds. This kept the motion on the weld pool surface slow enough to be captured as clearly as possible at 60 frames per second.

The weld pool patterns showed material being removed from the front of the weld pool, circulated around the sides of the pool and finally being deposited at the rear of the weld pool. Flows observed were from front to rear as indicated by Figures 30 through 32. The particles in this sequence move half the length of the weld pool in about $1/20$ of second or at an estimated speed of $.22\text{m/sec}$. Table X reviews selected reported speeds; however none of the speeds (except the present) are reported to be in a circumferential direction.

Figure 30 through 32 also show a thin layer of aluminum particles and other unidentified material dragging behind the weld pool. The layer is almost always present and



a. Time + 0 Seconds. Arc Moving From
Left to Right Direction of Weld



b. Time + 1.0 Seconds. Arc Extinguished.



c. Time + 2.0 Seconds. Weld Pool Depression Observable.



d. Time + 3.0 Seconds. Weld Pool Depression Observable.

Figure 28. Weld Pool Depression. 250A, 14.3 v, Welding Speed
.85 mm/sec. Actual Weld Pool Width of 11.1 mm.
Enlargement x4.0.



Figure 29. Solidified Weld Bead Showing 0.5 mm Rise at Center of Weld. 250A, 14.2 v, Welding Speed 4.17 mm/sec. Enlargement x3.2

is often highlighted with one large drop at the rear center of the weld pool.

TABLE X. REVIEW OF SELECTED REPORTED SPEEDS.

Investigator	Speed m/s	Comments
Present Investigation	.22	Using laser vision system, 2.58 Kw at 4mm Arc, 45° electrode tip, .85 mm/s welding speed HY80.
Saedi & Unkel [Ref. 4]	.05	Thermal fluid model 100 amp - report laminar flow
Zacharia et al. [Ref. 7]	.6-1.0	Three dimensional transient model - stationary and moving, .84 Kw, welding speed of 3.4 mm/sec 6061 aluminum
Kim & Na [Ref. 6]	.4	Numerical mapping model,, 2.0 Kw stationary welding AI5J 1042
Woods & Milner [Ref. 9]	.17	Experimental observation - simulated welds 160 amps - stationary

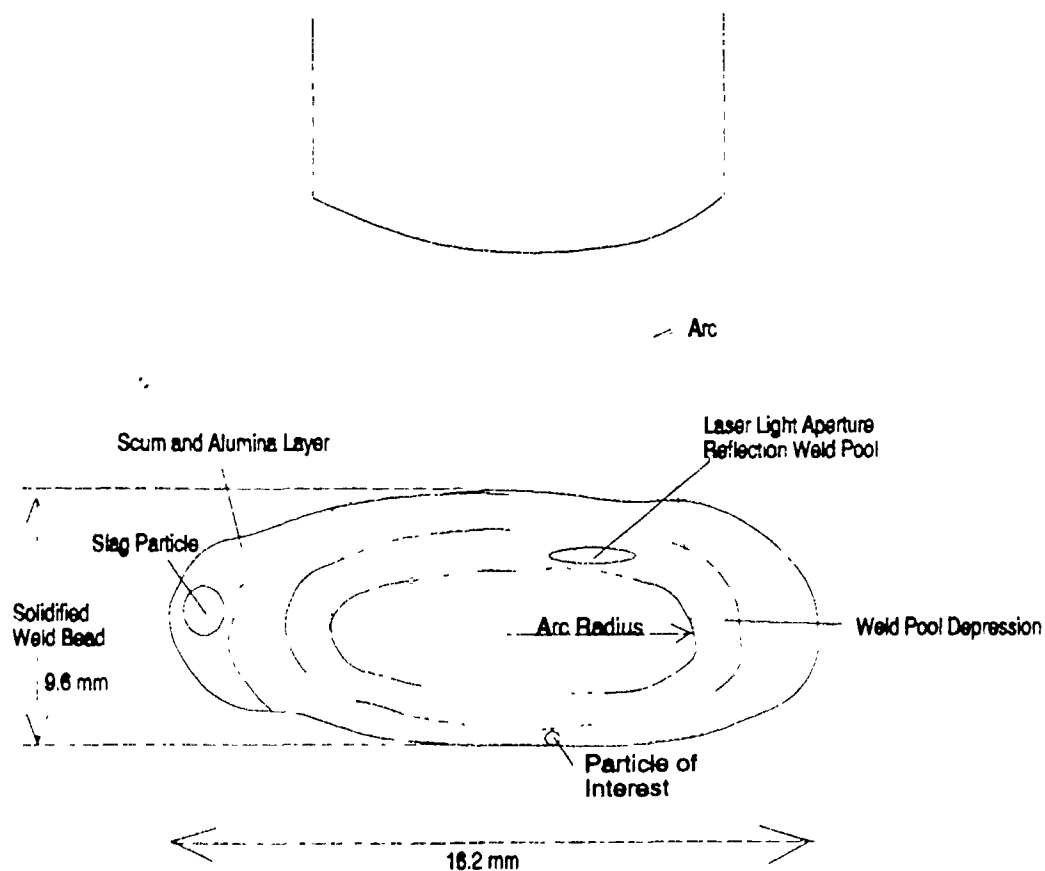
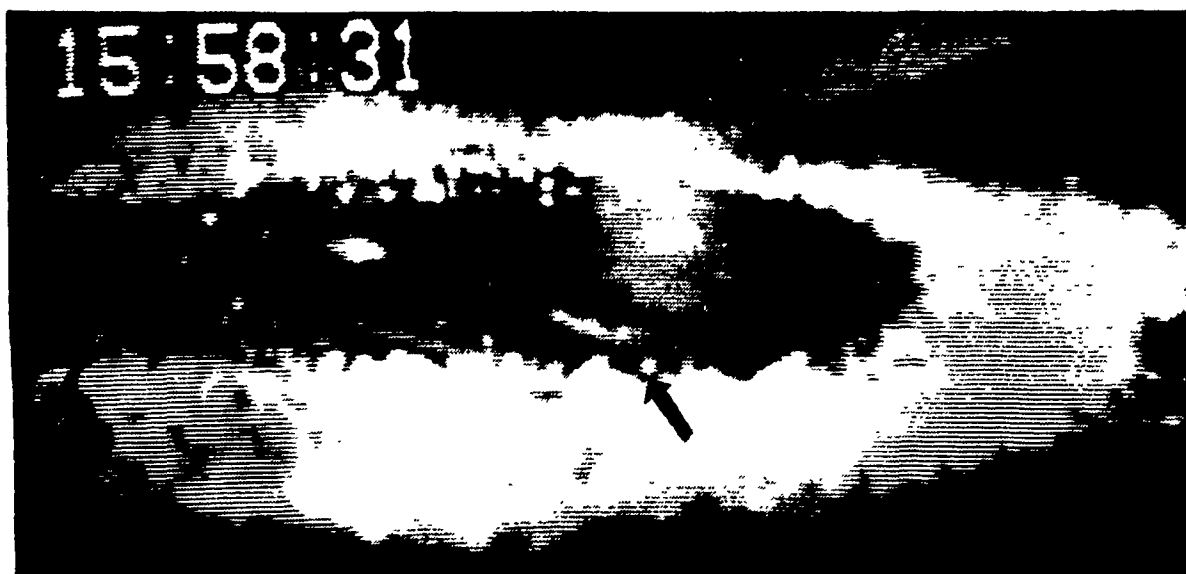


Figure 30. Weld Pool Flow. Time + 0 Seconds, 250 A, 14,2 v, Welding Speed 2.27 mm/sec. Enlargement x5.5.

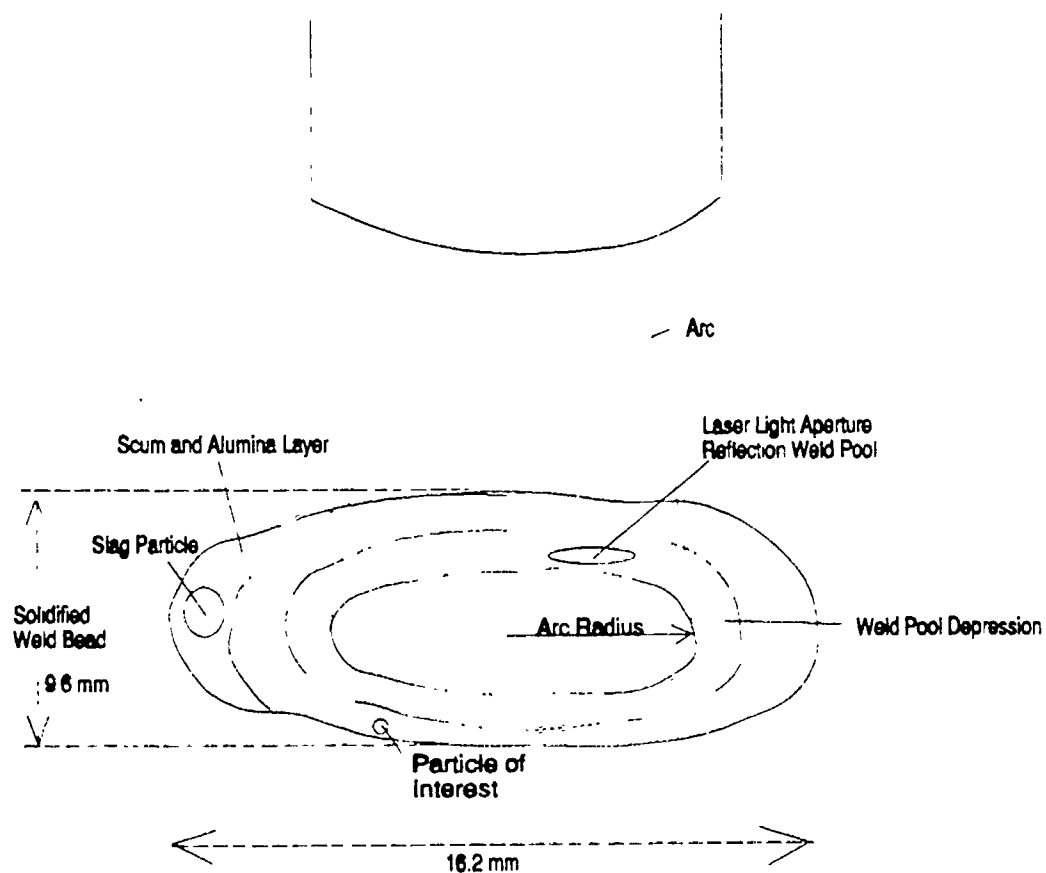


Figure 31. Weld Pool Flow. Time + .02 Seconds, 250 A, 14.2 v, Welding Speed 2.27 mm/sec. Enlargement x5.5.

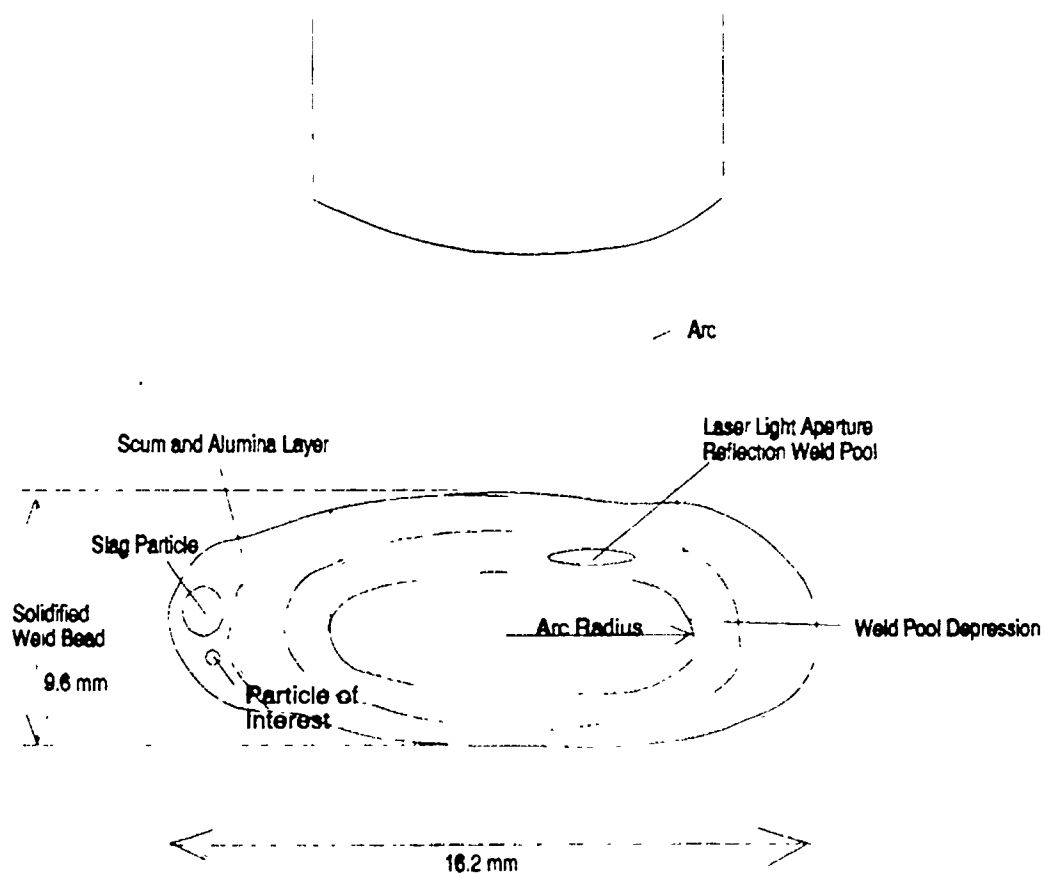


Figure 32. Weld Pool Flow. Time + .04 Seconds, 250 A, 14.2 v, Welding Speed 2.27 mm/sec. Enlargement x5.5.

V. CONCLUSIONS

Computational models describing convection and heat flow in weld pools are essential for the construction of a fully automatic welding system. The weld pool visualization system utilized in the present experiments has allowed a close and almost unobstructed view of the weld pool surface for both moving and stationary arc welds.

Under a wide variety of welding parameters for stationary welding, several main points are made. Firstly, weld pools are not flat as some models suggest, but rather rise about 1-2mm in height, decreasing the effective arc length. Weld pools also exhibit a free surface often shifting its height and crown formation. Secondly, weld pool rotation in the clockwise direction is not predicted by any numerical model to date and is not clearly reported in recent published experimental observations. Finally, weld pool oscillations are also not accounted for or predicted by any numerical model and are also not reported in any experimental studies. These features of the motion of the weld pool almost certainly have significant effect on the heat transfer in the pool.

Moving arc weld pool experiments using varying welding parameters have also shown several interesting features. These weld pools are characterized by a depression near the center of the pool and a rise in the tail end of the weld pool. This

free weld pool surface contains strong convection currents measured at .22m/sec. Pools also carry at their end impurities which become solidified at the center of the weld bead. Fluid flow in moving arc weld pools could be better photographed at shutter speeds higher than 60 frames per second.

LIST OF REFERENCES

1. Oreper, G.M., and Szekely, J., "Heat and Fluid-Flow Phenomena in Weld Pools," *Journal of Fluid Mechanics*, Vol. 147, pp. 63-76, 1984.
2. Kou, S., and Wang, Y.H., "Computer Simulation of Convection in Moving Arc Weld Pools," *Metallurgical Transactions A*, Vol. 17A, pp. 2271-2277, December 1986.
3. Wang, Y.H., and Kou, S., "Driving Forces for Convection in Weld Pools," *Advances in Welding Sciences and Technology*, p. 65, May 1986.
4. Saedi, H.R., and Unkel, W., "Thermal-Fluid Model for Weld Pool Geometry Dynamics," *Journal of Dynamic Systems, Measurement, and Control*, Vol. 111, pp. 268-276, June 1989.
5. Zacharia, T., Eraslan, A.H., Aidun, D.K., and David, S.A., "Three-Dimensional Transient Model for Arc Welding Process," *Metallurgical Transactions B*, Vol. 20B, pp. 645-659, October 1989.
6. Kim, S.D., and Na, S.J., "A Study on Heat and Mass Flow in Stationary Gas Tungsten Arc Welding Using the Numerical Mapping Method," *Journal of Engineering Manufacture*, Part B., pp. 233-242, 1989.
7. Zacharia, T., David, S.A., Vitek, J.M., and Debroy, T., "Weld Pool Development During GTA and Laser Beam Welding of Type 304 Stainless Steel, Part 1, Theoretical Analysis," *Welding Journal*, pp. 4995-5095, December 1989.
8. Ule, R.L., Joshi, Y., and Sedy, E.B., "A New Technique for Three-Dimensional Transient Heat Transfer Computations of Autogenous Arc Welding," *Metallurgical Transactions B*, Vol. 21B, pp. 1033-1047, December 1990.
9. Woods, R.A., and Milner, D.R., "Motion in the Weld Pool in Arc Welding," *Welding Journal*, pp. 163-173, April 1971.
10. Metcalfe, J.C., and Quigley, M.B.C., "Arc and Pool Instability in GTA Welding," *Welding Journal*, May 1977.

11. Bolstad, J.O., "Electronic Imaging Technique for Welding and Other High-Luminosity Processes," Informal report, Idaho National Engineering Laboratory, September 1987.
12. Kraus, H.G., "Experimental Measurement of Stationary SS 304, SS 316L and 8630 GTA Weld Pool Surface Temperatures," *Welding Journal*, July 1989.
13. Malinowski-Brodnicka, M., Ouden, G. den., and Vink, J.P., "Effects of Electromagnetic Stirring on GTA Welds in Austenite Stainless Steel," *Welding Journal*, pp. 525-595, February 1990.
14. Voelkel, D.D., and Mazumder, J., "Visualization of a Laser Melt Pool," *Applied Optics*, Vol. 29, no. 12, pp. 1718-1720, April 1990.
15. Stinchcomb, C., *Welding Technology Today, Principles and Practices*, Chapter 8, pp. 123-172, 1989.
16. *Owner's Welding Manual*, Form OM-210B, Miller Electronic Mfg. Co., January 1978.
17. *Ultra-Service Steels*, Industrial Information Bulletin, June 1990.
18. "System Description and Operating Instructions," *Laser-Augmented Welding Vision System*, Control Vision, Inc., Idaho Falls, Idaho.
19. *Model UV12 Nitrogen Laser Service Manual*, PRA Laser Inc., November 1987.
20. Rosenthal, D., "The Theory of Moving Sources of Heat and Its Application to Metal Treatments," *Transactions of the ASME*, November 1946.
21. Sedy, Eugene E., "Validation of a Computational Model for Autogenous Arc Welding," Master's Thesis, Naval Postgraduate School, Monterey, California, 1990.
22. Giedt, W.H., Tallerico, L.N., Fuerschbach, P.W., "GTA Welding Efficiency - Calorimetric and Temperature Field Measurements," U.S. Department of Energy, Contract Number DE-AC04-DP00789.
23. Niles, R.W., Jackson, C.E., "Weld Thermal Efficiency for the GTAW Process," *Welding Journal*, Vol. 54, pp. 265-325, 1975.

24. Giedt, W.H., "GTA Weld Penetration and Effects of Deviations in Machine Variables," Sandia National Laboratories Report, June 1987.

INITIAL DISTRIBUTION LIST

	No. of Copies
1. Defense Technical Information Center Cameron Station Alexandria, VA 22304-6145	2
2. Library, Code 52 Naval Postgraduate School Monterey, CA 93943-5002	2
3. E.A. Metzbower Naval Research Laboratory Washington, D.C. 20375-5000	1
4. Department Chairman, Code 69 Department of Mechanical Engineering Naval Postgraduate School Monterey, CA 93943-5000	1
5. Yogendra Joshi, Code ME/Ji Naval Postgraduate School Monterey, CA 93943-5000	2
6. Richard Morris Code 2815 David Taylor Research Laboratory Annapolis, MD 21402	1
7. RADM Roger Horne SEA-05 Naval Sea Systems Command Washington, D.C. 20362-5101	1
8. RADM Thomas W. Evans SEA-92R Naval Sea Systems Command Washington, D.C. 20362-5101	1
9. Naval Engineering Curricular Office Code 34 Naval Postgraduate School Monterey, CA 93943-5000	1

10. Daniel C. Espinosa
3601 N.E. Liverpool Drive
Bremerton, WA 98310

3